Clays and Clay Minerals, Vol. 63, No. 4, 290–310, 2015.

REACTIVITY OF CALLOVO-OXFORDIAN CLAYSTONE AND ITS CLAY FRACTION WITH METALLIC IRON: ROLE OF NON-CLAY MINERALS IN THE INTERACTION MECHANISM

Camille Rivard[1,2], Manuel Pelletier[1,2], Nicolas Michau[3], Angelina Razafitianamaharavo[1,2], Mustapha Abdelmoula[4,5], Jaafar Ghanbaja[6], and Frédéric Villiéras[1,2]

[1] Université de Lorraine, LIEC, UMR7360, Vandœuvre-lès-Nancy, F-54500, France
[2] CNRS, LIEC, UMR7360, Vandœuvre-lès-Nancy, F-54500, France
[3]Andra, 1/7 rue Jean Monnet, Parc de la Croix Blanche, Châtenay-Malabry Cedex, F-92298, France
[4] Université de Lorraine, LCPME, UMR7564, Vandœuvre-lès-Nancy, F-54500, France
[5] CNRS, LCPME, UMR7564, Vandœuvre-lès-Nancy, F-54500, France
[6] Université de Lorraine, IJL, Nancy, F-54000, France

Abstract—In order to better understand the possible interactions between steel canisters and a claystone host rock, in this case the Callovo-Oxfordian rock (COx), the present study investigated in detail, under conditions relevant to high-level radioactive waste repositories (anoxic conditions, temperature of 90ºC), the reactions between metallic iron and: (1) COx; (2) the clay fraction extracted from COx (CF); and (3) mixtures of CF with quartz, calcite, or pyrite. Batch experiments were then carried out in the presence of NaCl-$CaCl_2$ background electrolyte, for durations of 1, 3, and 9 months. Solid and liquid end-products were characterized by a combination of techniques including liquid analyses, transmission and scanning electron microscopies, X-ray diffraction, N_2 adsorption at 77 K, and Mössbauer spectroscopy. The interaction between CF and metallic iron appeared to proceed by means of pathways similar to those illustrated in previous studies on interactions between metallic iron and purified clays. In spite of the many similarities with previous studies, significant differences were observed between the behavior of COx and CF, particularly in terms of pH and Eh evolution, iron consumption, chemical composition of the neoformed particles, and textural evolution. Such differences demonstrate the important role played by non-clay minerals in reaction pathways. The addition of carbonates or pyrite to CF did not lead to significant change in reactivity. In contrast, under the conditions used in the present study, *i.e.* for relatively low iron:clay ratios, the presence of quartz strongly influenced reaction pathways. In the presence of quartz, magnetite was observed only in trace abundances whereas the amounts of magnetite were significant in experiments without quartz. Furthermore, filamentous serpentine particles with a small Al:Si ratio appeared which could develop from an FeSiAl gel that only forms in the presence of quartz. Considering that most clay rocks currently being considered for radioactive waste disposal contain significant amounts of quartz, the results obtained in the present study may be of significant interest for predicting the long-term behavior of clay barriers in such sites.

Key Words—Clay–iron Reaction, Claystone, Metallic Iron, Quartz.

INTRODUCTION

The host rock selected by the French national radioactive waste management agency (ANDRA) for a potential underground radioactive waste disposal site near Bure, France, is the COx. This rock is made up of ~50% of clays minerals: illite, interstratified illite-smectite, chlorite, and kaolinite (Rousset, 2002; Brégoin, 2003; Gaucher *et al.*, 2004; Yven *et al.*, 2007), with the remaining fraction consisting mainly of quartz, calcite, dolomite, feldspars, and pyrite. Under storage conditions, this rock will be subjected to changes in water activity and to temperatures up to 90ºC resulting from nuclear reactions in High-Level radioactive Waste (HLW), while interacting with various barrier materials such as concrete, glass, and steel (Landais, 2006). These changes will mainly occur at the interface between the rock and the iron canister surrounding the vitrified radioactive waste. Understanding the various transformations occurring when the COx and metallic iron are placed into contact with one another under conditions close to those that will occur in the radioactive waste storage is therefore of prime importance.

Numerous studies have focused on the reaction of metallic iron with individual clay phases such as smectite (Garfield, SWa-1, Drayton, CP4, SbId, SbS-I, SWy-2, SAz-1, SapCa-2, and SapFe08 in Lantenois *et al.*, 2005; Kunipia F in Ishidera *et al.*, 2008; SAz-1, STx-1, SBCa-1, SCa-3, and SWa-1 in Osacky *et al.*, 2010; Garfield, SbId, and SWy-2 in Lanson *et al.*, 2012; SHCa-1, SAz-1, SWy-1, STx-1, and SWa-1 in Balko *et al.*, 2012), illite (Perronnet, 2004), or kaolinite (Kohler, 2001; Perronnet, 2004; Rivard *et al.*, 2013a, 2013b) as well as on the interaction between metallic iron and

* E-mail address of corresponding author:
rivard.camille@gmail.com
DOI: 10.1346/CCMN.2015.0630404

bentonite[1] (FoCa7 in Habert, 2000 and Perronnet *et al.*, 2008; MX-80 in Guillaume *et al*., 2003, 2004, Charpentier *et al.*, 2006, Mösser-Ruck *et al.*, 2010, Savage *et al,.* 2010, and Jodin-Caumon *et al.*, 2010; Kunigel V1 bentonite in Wilson *et al.*, 2006 and Ishidera *et al.*, 2008).

Most previous studies revealed significant oxidation of metallic iron, destabilization of clay phases, and formation of Fe-rich serpentine and magnetite. Under conditions relevant to HLW storage, smectite, illite, and kaolinite were shown to be reactive with metallic iron (Rivard, 2011; Rivard *et al.*, 2013a). The presence of those minerals results in a significant oxidation of metallic iron, leading to the formation of new Fe-rich clay minerals. In the case of kaolinite, berthierine is shown to be the dominant product; it precipitates in an epitaxial relationship with the initial kaolinite particles, and smaller amounts of other Fe-serpentines (greenalite and cronstedtite) are also observed (Rivard, 2011; Rivard *et al.*, 2013a). When illite and smectite were the starting materials, evidence of epitaxial growth of Fe-serpentine was not unambiguous, but serpentine precipitation was observed leading to filamentous or needle-shaped products in some studies (Lantenois, 2005; Rivard, 2011) and conical and pyramidal crystals in other works (Pignatelli *et al*., 2013).

In parallel to these investigations on pure minerals, studies were also carried out to assess the mineralogical transformations of COx rock in the presence of metallic iron and under anoxic atmosphere. Batch experiments in which ground COx was in contact with either powdered metallic iron or iron foils were thus performed at 90ºC. Those experiments showed that the main clay minerals involved in corrosion processes are illites and interstratified illite-smectites, and revealed the precipitation of Fe-serpentines in the system (de Combarieu *et al.*, 2007). Batch experiments with powdered iron also revealed a strong influence by both the liquid:solid and iron:clay ratios. For instance, Pierron (2011) showed that an increase in the liquid:solid ratio led to a greater degree of destabilization of illite and illite-smectite and an enhanced formation of Fe-rich 7 Å phases. The specific surface area (SSA) of metallic iron also has a crucial influence on iron−clay interaction by affecting the reaction pathway and because of the ambient physico-chemical parameters of the medium (Bourdelle *et al*., 2014). Experiments mimicking the situation encountered in waste disposal sites were also performed by placing a heated iron rod (90ºC) in direct contact with COx rock (Schlegel *et al.*, 2008). In that case, the formation of one layer of magnetite together with one layer of Fe-phyllosilicates and Ca-rich siderite is observed at the interface between iron and COx.

As far as the present authors are aware, no study has analyzed in detail the reactivity of the clay fraction (referred to hereafter as CF) of COx toward metallic iron, because previous publications have focused either on raw COx or pure clay phases. In that context, the aim of the present study was two-pronged: (1) to analyze the reactivity of the CF of the COx because the characteristics of the clay minerals present could have some influence on their reactivity; and (2) to analyze the role of the non-clay minerals in the reactivity of the material as a whole. Previous studies such as that of de Combarieu *et al.* (2007) have shown that, upon reaction of COx with metallic iron at 90ºC, quartz and feldspar are destabilized, possibly due to a large pH increase, whereas calcite and muscovite remained stable. Precise quantitative information on the role of each mineral in the reaction has yet to be established. Carbonates (calcite and dolomite) could have a significant effect on the evolution of the reaction through a modification of the physicochemical equilibrium, due to their role in pH buffering. The system could also be influenced by the presence of quartz, feldspar, and pyrite that could provide additional sources of Si and Fe. Using experimental conditions similar to those used by Rivard *et al.* (2013a) (anoxic atmosphere, NaCl-$CaCl_2$ solution, 90ºC), the present study compares the results obtained by reacting metallic iron with COx rock, the CF extracted from the COx rock, and mechanical mixtures of CF with quartz, calcite, and pyrite.

MATERIALS AND METHODS

Starting material

COx rock (Bure, France) was extracted by deep bores from the Callovo-Oxfordian formation that extends over a thickness of 130 m between depths of 422 and 552 m. COx rock contains ~50% of clay minerals (illite, interstratified illite-smectite, chlorite, and kaolinite), with the remaining fraction consisting of silicates (quartz, K-feldspar, plagioclase, and mica), carbonates (calcite, dolomite, siderite, and ankerite), pyrite, sulfates, phosphates, and organic matter. Numerous studies have investigated the COx formation and have suggested both vertical and lateral variability in terms of composition (Rousset, 2002; Brégoin, 2003; Gaucher *et al.*, 2004; Yven *et al*., 2007).

The sample used for in-depth study in this project was collected from the lithological unit C2b1 at a depth of ~490 m in the interest zone (D. Guillemot, Andra report KMFIAEAP090002, 2009). This sample was located close to the transition zone between the zone where R = 0 (disordered illite-smectite (I-S) with 40−60% smectite) is dominant and the zone where R = 1 (ordered I-S with 20−50% smectite) is dominant. The

[1] The use of bentonite in numerous studies was mainly guided by the fact that, in some countries, the concept for HLW storage included the presence of an additional engineered bentonite barrier between the canister and the host rock.

https://doi.org/10.1346/CCMN.2015.0630404 Published online by Cambridge University Press

sample was made up of large blocks 20 to 30 cm long of broken core from the EST26456 (FOR 1118) deep bore. The samples were not protected from exposure to O_2 during drilling and storage. The SSA, determined by applying the Brunauer-Emmet-Teller (BET) method (Brunauer *et al.*, 1938) to N_2 adsorption data of the COx sample used in the present study, was 36.4 ± 0.9 m^2/g. The cation exchange capacity (CEC), determined using the hexamine cobalt(III) exchange method was 15.6 ± 0.5 meq/100 g (Rivard, 2011). The X-ray diffraction (XRD) patterns collected from clay samples prepared and examined as described below (Figure A in supplementary material, deposited with the Editor in Chief and available at http://www.clays.org/JOURNAL/JournalDeposits.html) confirmed the presence of interlayered illite-smectite, illite, kaolinite, and chlorite.

The non-clay minerals used in the present study (quartz, calcite, and pyrite) were chosen according to their purity and grain size, consistent with those of COx rock. The quartz was of sedimentary origin (Entraigues, France; Poirier, 1984) and provided by SIFRACO (Nemours, France). Calcite was provided by SPT (Six-Four-les-Plages, France) from an unknown deposit. Pyrite was collected from a hydrothermal deposit in Peru (Ačai *et al.*, 2009). The d_{50} values for these minerals, determined using a laser-diffraction particle-size analyzer (Helos, Sympathec, Clausthal-Zellerfeld, Germany), were 90, 224, and 100 μm, for quartz, calcite, and pyrite, respectively. Their SSAs were negligible (~0.1 ± 0.2 m^2/g)) compared with that of the COx.

Powdered metallic iron (α-Fe) (purity ⩾99.5%, average grain size = 40 μm, SSA = 0.1 ± 0.1 m^2/g) was provided by Aldrich (Saint-Louis, Missouri, USA). In agreement with previous studies (Guillaume, 2002; Guillaume *et al.*, 2003, 2004; Mosser-Ruck *et al.*, 2010; Jodin-Caumon *et al.*, 2010, 2012) the composition of the chloride solution (NaCl: 0.0207 mol.kg^{-1}, $CaCl_2$: 0.0038 mol.kg^{-1}) used in the present study was chosen as a proxy for natural pore water from the COx formation and stored under N_2 atmosphere (O_2 and H_2O <1 ppm).

Experimental procedure

CF extraction. The procedure to extract the CF was designed to remove non-clay minerals while preserving the full spectrum of clay minerals of all particles sizes (*i.e.* no selective extraction of the <2 μm fraction). No protective measure against oxidation was taken for the CF extraction procedure. Large COx blocks were first crushed into smaller fragments (1−2 cm), dispersed for 48 h in pure water, and sonicated for 10 min. The suspension was wet-sieved at 32 μm to remove coarse impurities such as large quartz and calcite grains or pyritized ammonites. The <32 μm size fraction suspension was then dried at 80ºC and hand-ground gently in an agate mortar. The resulting powder was dispersed at a solid concentration of 40 g/L in sodium acetate (CH_3COONa, 1 M) for 12 h. The suspension pH was adjusted to pH = 5 by addition of acetic acid (CH_3COOH) and the suspension was heated at 80ºC for 2 h while stirring. The suspension was then exchanged three times in 1 M NaCl and dialyzed in MilliQ water (Merck) until the supernatant was chloride-free as determined by conductivity measurements (<4 μS/m). The final suspension was stirred, sonicated, and centrifuged at 35,000 × *g* for 90 min. Settled particles were freeze-dried before being hand-ground in an agate mortar. The XRD pattern of the final product (Figure B in the supplementary material) revealed an increase in the relative intensity of clay peaks and also confirmed the presence of small amounts of quartz. According to observations by transmission electron microscopy (TEM) (not shown), these remaining quartz particles were <2 μm in size and could not be removed from the CF without affecting the integrity of the clay particles' size distribution. The SSA of the CF was 99 ± 2 m^2/g and its CEC was 25 ± 1 meq/100 g.

Protocol. Iron:clay and solution:clay mass ratios were fixed at 1:3 and 20:1, respectively (see Rivard *et al.*, 2013a for the justification of these values). Accordingly, 6 g of the CF was introduced into the reactors with 2 g of metallic iron and 120 mL of chloride solution. All the other experiments were designed with the same mass of metallic iron (2 g) and taking into account the following average composition for COx; 50% of clay minerals, 24.5% of quartz, 24.5% of calcite, and 1% of pyrite. Consequently, in order to maintain constant iron:clay and solution:clay ratios, experiments with COx were carried out with 12 g of rock whereas experiments on mixtures were carried out by adding 2.94 g, 2.94 g, or 0.12 g of quartz, calcite, or pyrite, respectively, to the 6 g of CF (Table 1). This obviously led to varying mineral:solution and mineral:iron mass ratios.

Mineral powders (clays and non-clay minerals) were stored overnight in an oven at 80ºC. For experiments involving COx, the rock was previously ground finely in a tungsten carbide mortar of a mechanical grinder. Oxygen was removed from the chloride solution by bubbling N_2 for 1 h. Samples were then conditioned in an M. Braun (Garching, Germany) Labstar glove box, under N_2 atmosphere (O_2 and H_2O <1 ppm). Minerals, metallic iron, and solution were introduced in Parr (Moline, Illinois, USA) autoclaves (equipped with a polytetrafluoroethylene liner), mixed, and kept at 90ºC for 1, 3, or 9 months. The nomenclature of the samples in Table 2 includes sample and experimental information. Blank experiments without iron were used as controls. At the end, the reactors were quickly cooled and opened under N_2 atmosphere. Solid and liquid phases were separated by centrifugation (46,000 × g for 45 min). Solid fractions were freeze-dried, ground gently

https://doi.org/10.1346/CCMN.2015.0630404 Published online by Cambridge University Press

Table 1. Minerals proportions (g, mass %), liquid:minerals ratio, and Fe:minerals ratio in the three sets of experiments.

	COx rock		Clays		Quartz		Calcite		Pyrite		Liquid: minerals ratio	Fe: minerals ratio
	g	%	g	%	g	%	g	%	g	%		
COx	12	100									10	0.16
CF	–	–	6	100	–	–	–	–	–	–	20	0.33
CF+quartz	–	–	6	67	2.94	33	–	–	–	–	13	0.22
CF+calcite	–	–	6	67	–	–	2.94	33	–	–	13	0.22
CF+quartz+calcite	–	–	6	50	2.94	25	2.94	25	–	–	10	0.17
CF+pyrite	–	–	6	98	–	–	–	–	0.12	2	20	0.33

in an agate mortar, and stored under N_2 atmosphere. Solutions were filtered at 0.2 μm, acidified by nitric or hydrochloric acid, and frozen.

Characterization of the products

Liquid-phase characterization. pH and Eh measurements of the supernatants were carried out under anoxic atmosphere (glove box under N_2 atm; O_2 and H_2O <1 ppm), at room temperature, using an Ag/AgCl pH electrode (VWR, RADNOR, Pennsylvania, USA) and a SentixORP electrode (WTW, Weilheim, Germany). The initial state was measured on a clay/experimental-solution mixture, in identical proportions to the reactive systems. The chemical composition (Na, Mg, Al, Si, K, Ca, and Fe_{tot}) of each solution was measured using inductively coupled plasma optical emission spectrometry on HNO_3-acidified supernatants. The amount of Fe^{2+} cations was measured using a Shimadzu (Duisburg, Germany) UV-2501PC spectrophotometer on a parallel (HCl-acidified) aliquot after reaction with 1,10-phenanthroline.

Solid-phase characterization. For analysis by scanning electron microscopy (SEM) of the coarsest fractions, the bulk sample was subjected to successive ultrasonic treatments and sedimentation in alcohol until a particle-free supernatant was obtained. Remaining grains were dried under N_2 atmosphere, placed on carbon adhesive tabs mounted on a stub of metal, and carbon coated. Grains were also embedded in an organic polymer (Epon 812, EMS, Hatfield, Pennsylvania, USA) and prepared as polished sections. The SEM images were obtained using an Hitachi FEG S-4800 microscope equipped with a cold cathode, running at 1−10 keV, and under vacuum (10^{-4} Pa in the specimen chamber). The micrographs were recorded in secondary- or backscattered-electron modes, with a spatial resolution of 1 nm. The energy-dispersive X-ray spectrometer (EDS, Thermo Scientific Noran system) was also used to obtain semi-quantitative chemical analyses coupled to the SEM images.

For TEM analysis of fine fractions, 10 mg of powder was dispersed in ethanol and treated ultrasonically for 5 min. One drop of suspension was placed on a carbon-coated copper grid and evaporated. The TEM images were acquired using a CM20 Philips (Eindhoven, The Netherlands) microscope equipped with a LaB_6 filament, running at 200 kV and under vacuum. Images were recorded using a CCD camera. Chemical compositions were determined using an EDS spectrometer (PGT, Princeton, New Jersey, USA) equipped with an ultrathin window (Si-Li) X-ray detector. The analysis was carried out in nanoprobe mode with a probe diameter of 10 nm. For each reacted sample, at least 20 analytical points were recorded on isolated particles. Counting time was ~40 s with a dead time of between 10 and 50%. High-resolution TEM images were also obtained by embedding samples in an organic polymer (Epon 812) and subsequent ultramicrotoming of ultrathin sections (50−90 nm thick). The slices were placed on a carbon-coated copper grid and observed at high magnification (× 200,000).

N_2 adsorption-desorption isotherms at 77 K were recorded on a step-by-step automatic setup built in the Laboratoire Interdisciplinaire des Environnements

Table 2. Sample nomenclature.

	Without iron	With iron
Callovo-Oxfordian (COx)	*x*m	*x*m-Fe
Clay fraction of the Callovo-Oxfordian (CF)	*x*m-CF	*x*m-Fe-CF
CF with added non-clay minerals	*x*m-CF+mineral	*x*m-Fe-CF+mineral

x corresponds to the duration of the experiment (1, 3, or 9 months) and mineral corresponds to the non-clay mineral added (quartz, calcite, or pyrite).

https://doi.org/10.1346/CCMN.2015.0630404 Published online by Cambridge University Press

Continentaux (Vandœuvre-lès-Nancy, France). Prior to N_2 adsorption experiments at 77 K, samples were outgassed at 110ºC for 18 h under a residual vacuum of 0.01 Pa. The SSA values were determined by applying the BET equation (Brunauer *et al*., 1938) using 16.3 $Å^2$ as the cross-sectional area of N_2 molecules.

Bulk samples were analyzed by XRD using 1 g of randomly oriented powder, placed on a rotating sample holder, and leveled with a glass slide to obtain a flat surface. Additional XRD data were acquired from a second set of randomly oriented bulk-sample mounts using zincite (ZnO) as an internal standard. In this second preparation, samples (1 g) were first mixed with 0.111 g of ZnO and ground in an agate mortar for 5 min. Oriented mounts were analyzed after decarbonation and extraction of the fine fraction. The sample (1 g of COx or 0.5 g of samples after reaction) was dispersed in 100 mL of ultrapure water. Suspension pH was adjusted to pH = 4 by addition of a 0.5 M HCl solution. The suspension was then rinsed three times with ultra-pure water dispersion and centrifugation cycles at $46{,}000 \times g$ for 45 min were repeated. The settled particles were dispersed in 80 mL of ultra-pure water, stirred, sonicated, and then left to settle again. A portion of the suspended sediment containing the <2 μm fraction was sampled according to Stokes law and then centrifuged at $46{,}000 \times g$ for 45 min. The settled particles were dispersed in 5 mL of ultrapure water, sonicated, and the paste obtained was spread on three glass slides. The oriented preparations were air-dried; one slide was solvated with ethylene-glycol and another heated at 550ºC.

X-ray diffraction patterns were collected on a D8 Advance Bruker AXS (Karlsruhe, Germany) diffractometer in θ-2θ geometry equipped with a LynxEye fast linear detector using CoKα radiation (λ = 0.17903 nm) at 35 kV and 45 mA. Intensities were recorded from 3 to 64º2θ with a 0.035º2θ step size using a 3 s counting time per step for randomly oriented powder without standard, from 2 to 40º2θ with a 0.035º2θ step size using a 3 s counting time per step for randomly oriented powder with standard, and from 4 to 80º2θ with a 0.02º2θ step using a 3 s counting time per step for oriented mounts. Data reduction and analysis were performed with the *EVA* software (*DIFFRACplus* from Bruker) and diffraction peaks were identified by comparison with powder diffraction files (PDF2 database from the International Center for Diffraction Data).

Transmission ^{57}Fe Mössbauer spectra were collected using a 50 mCi source of ^{57}Co in rhodium. Bulk powder samples were placed in a sample holder under He atmosphere and then placed quickly in the cryostat at high vacuum (10^{-6} mbar). Spectrometer calibration was performed using a 25 μm foil of α-Fe at room temperature. Spectra were acquired at room temperature (295 K) and spectral adjustments were performed using Lorentzian-shaped lines.

RESULTS

Solutions characterization

pH and Eh evolution. Dispersion of COx in the experimental solution (with Na and Ca cations only) led to a pH value of 8.3 due to the presence of carbonates that buffered the solution (Figure 1a; numerical value in Table A of supplementary material). This value agrees with that measured experimentally by de Combarieu *et al.* (2007) and is higher than that modeled by Beaucaire *et al*. (2012) (pH of 6.16). This latter difference could be attributed largely to the measurement conditions (25ºC, under N_2 atmosphere in the present study compared with 80ºC and a CO_2 partial pressure of $10^{-0.36}$ atm in Beaucaire *et al.*, 2012). The negative Eh value (−200 mV, Figure 1c) indicated that, despite the lack of protection against O_2 during core sampling, COx rock was not oxidized completely. *x*m samples yielded lower pH values than the equilibrated solution (7.8 for 1 month) but were still buffered. Eh values remained negative and slightly higher than in the equilibrated solution (between −105 and −60 mV). pH values for *x*m-Fe were slightly higher than those for *x*m but close to that measured on the initial equilibrated solution. In that case, Eh values exhibited a strong decrease after 1 month (−190 to −285 mV for 1m-Fe) and remained relatively stable over time. Higher pH values and lower Eh values were obtained by de Combarieu *et al.* (2007). The larger Fe:COx ratio used by those authors was probably responsible for the larger increase in pH values and decrease in Eh values.

Equilibration of CF with the experimental solution led to a pH of 4.2 and an Eh of 180 mV. Values obtained for *x*m-CF remained quite stable over time. Addition of metallic iron (*x*m-Fe-CF samples) led to much higher pH values (~10) which remained constant with increasing time. Eh values were negative and decreased regularly down to ~−400 mV for 9m-Fe-CF.

The addition of minerals to CF did not change the pH value in the case of quartz, but led to a slight increase (+0.5) in the case of pyrite, and led to a strong increase towards pH 8 in the case of calcite that clearly exhibited a buffering effect (Figure 1b). No time evolution was observed for any mineral addition. When metallic iron was added to the system, whatever the mineral, after 1 month, the pH increased significantly to a value between 9.2 and 10. This value remained constant over time in the case of pyrite or calcite, whereas in the presence of quartz, the pH values decreased with time to reach values of ~8 after 3 months of reaction. Except for quartz, initial Eh values appeared to be affected by the addition of minerals to the CF, as calcite and pyrite led to Eh values of 55 and −21 mV, respectively (Figure 1d). All these values changed slightly with increasing time. Addition of metallic iron to the samples led to significant Eh decreases which were close to those observed in the case of pure CF.

https://doi.org/10.1346/CCMN.2015.0630404 Published online by Cambridge University Press

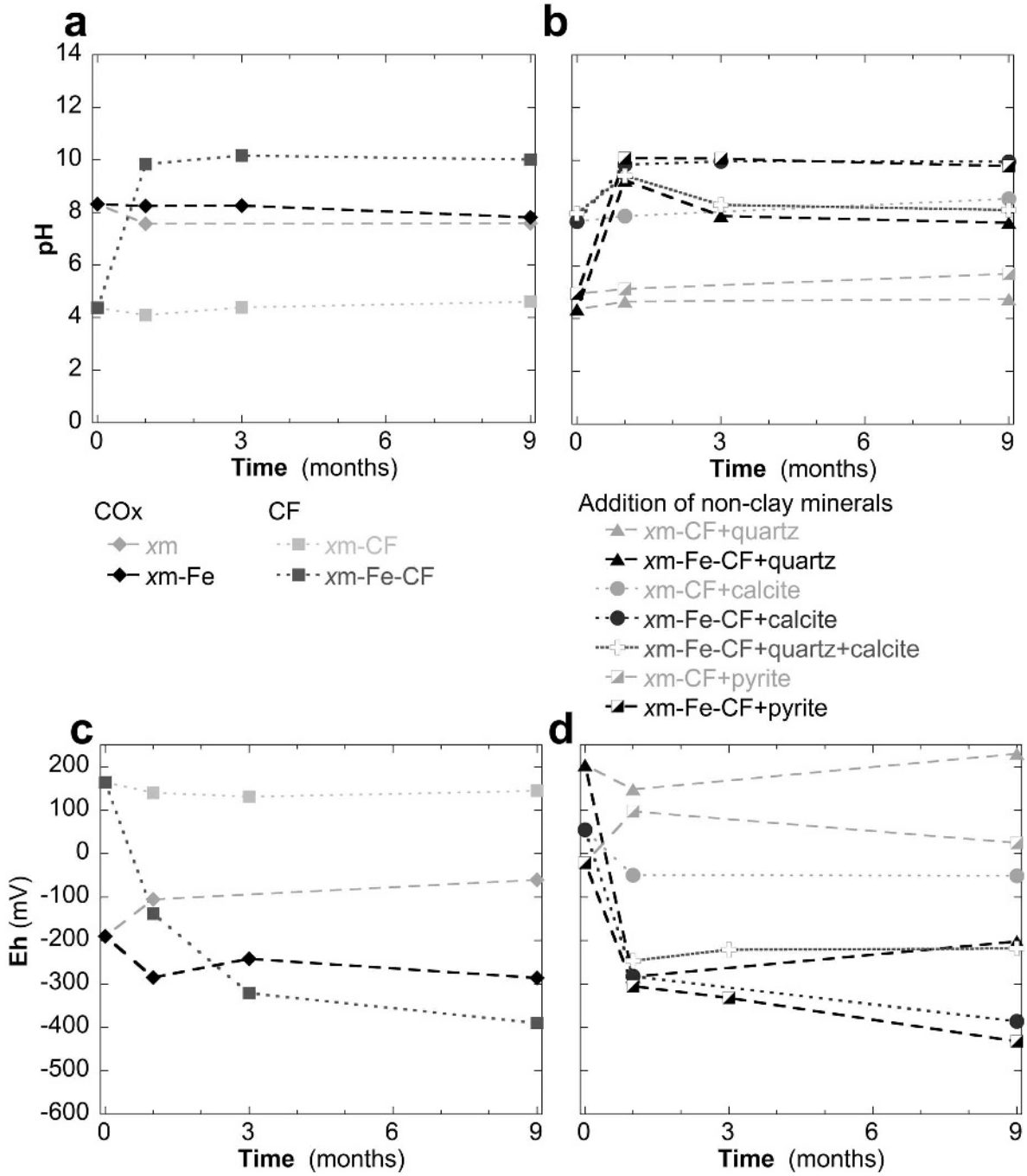

Figure 1. pH (a, b) and Eh (c, d) evolution of COx and CF supernatants, in the presence and in the absence of metallic iron, with or without the addition of non-clay minerals, as a function of time.

Cation concentrations in solution. Concentrations of Na, Mg, Al, Si, K, Ca, and Fe were measured in the supernatants (values are given in Table A of the supplementary material; and values for K, Mg, and Ca concentration evolution are given in Figure 2). Aluminum was not detected in any of the solutions investigated (detection limit: 1 mg/L). Initial values measured after 24 h of equilibrium between the various minerals and the starting solution provided information on the exchange between the solids and the solution introduced. A comparison between initial values for COx and for CF revealed smaller amounts of K, Mg, and Ca in the CF. This could be attributed to the absence of calcite, feldspar, and dolomite in the CF and this was confirmed by initial values obtained for initial CF+calcite samples that were significantly richer in Ca. The time evolution of these

https://doi.org/10.1346/CCMN.2015.0630404 Published online by Cambridge University Press

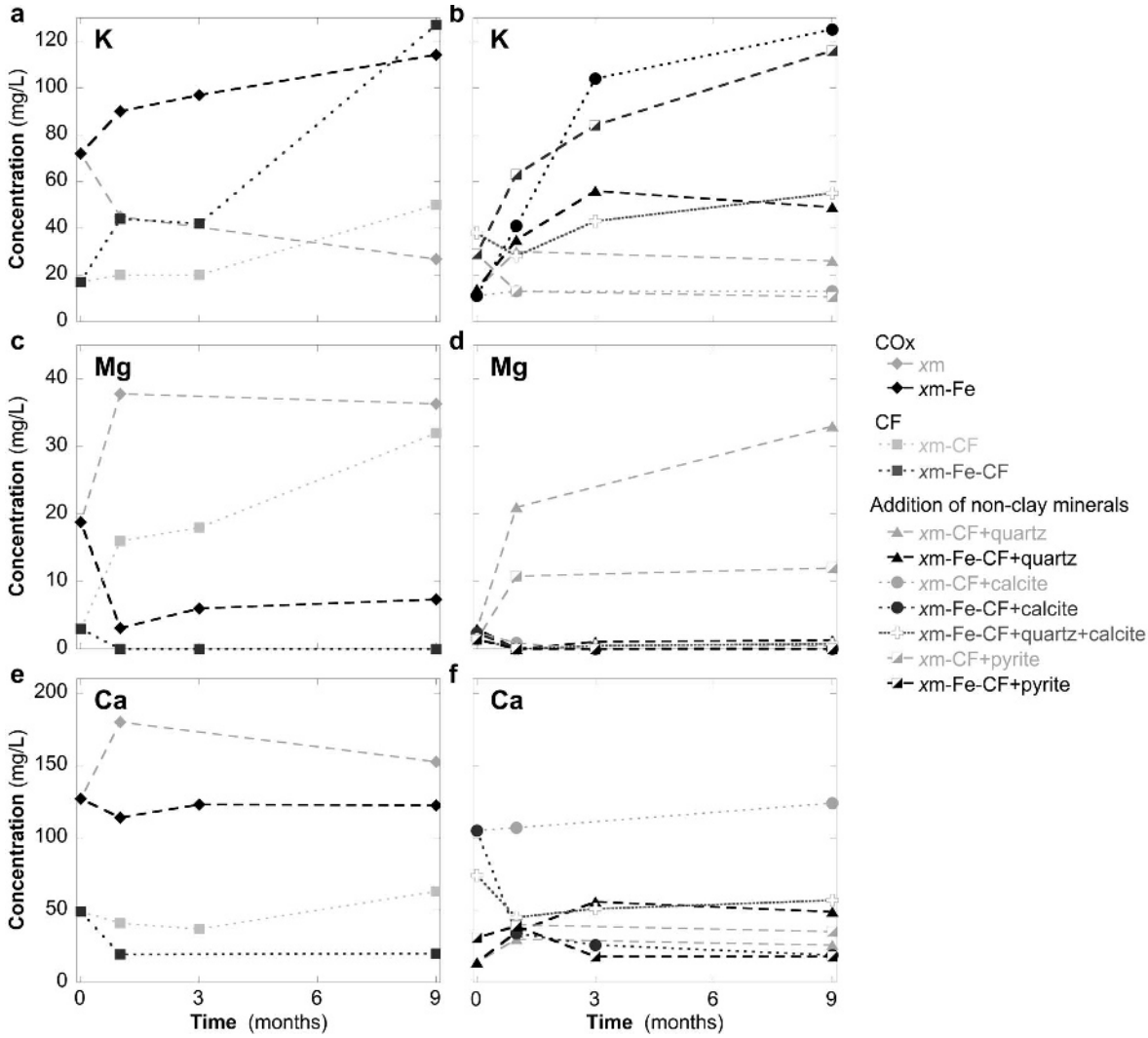

Figure 2. K, Mg, and Ca cations concentrations in COx and CF supernatants (a, c, e) in the presence and in the absence of metallic iron, with or without the addition of non-clay minerals (b, d, f), as a function of time.

concentrations provided information about the reactions occurring upon heating in anoxic atmosphere. In the case of COx, the Mg and Ca contents increased with time over the first month of reaction whereas those of K and Si decreased. In the case of the CF, the patterns were not the same because the evolution appeared to be slower with an increase in K, Ca, and Mg between 3 and 9 months of equilibration. The addition of various minerals to the CF did not modify significantly the above-described patterns except for the addition of pyrite which led to increased Fe concentrations, and of calcite which, logically, led to greater Ca concentrations.

Upon addition of metallic iron to the various systems, significant changes were observed indicating that different reactions were occurring in the system. For all investigated mineral compositions, Mg was almost eliminated from the solution after reaction with metallic iron, which suggested the formation of new solid phases containing this element. In contrast, the K concentration in the solutions increased significantly, revealing the increased dissolution of K-bearing phases under such conditions. In that case, the addition of quartz seemed to reduce the dissolution rate of K for one or more K-bearing minerals because lower values were obtained in the presence of this mineral. As far as Ca is concerned, the general trend was a moderate decrease in its concentration. Finally, in all cases other than 9m-Fe, which exhibited a slightly larger value, the Fe contents of the solutions were extremely small; this suggested that if Fe reacts with the various minerals, it must be incorporated immediately into solid phases.

Solid-phase analyses

The morphological changes between initial components of the mixture and the end-product were first analyzed by combining microscopy techniques and N_2

https://doi.org/10.1346/CCMN.2015.0630404 Published online by Cambridge University Press

adsorption-desorption isotherms. The results of XRD analyses were then presented and the neoformed Fe-bearing clay phases were characterized using high-resolution TEM (HRTEM), TEM-EDS analyses, and Mössbauer spectroscopy.

Morphological changes. Whereas COx, CF, *x*m, and *x*m-CF samples were light brown, *x*m-Fe and *x*m-Fe-CF solid end-products displayed a green-brown color, suggesting the presence of a mixture of ferrous and ferric iron.

Observations by SEM and EDS analyses of the coarsest fraction of *x*m-Fe samples showed the presence of aggregates, 10−100 μm in size. Three different types of aggregates were identified: (1) clay aggregates; (2) metallic iron grains partially covered by a thin and discontinuous layer of phyllosilicates (Figure 3b), the

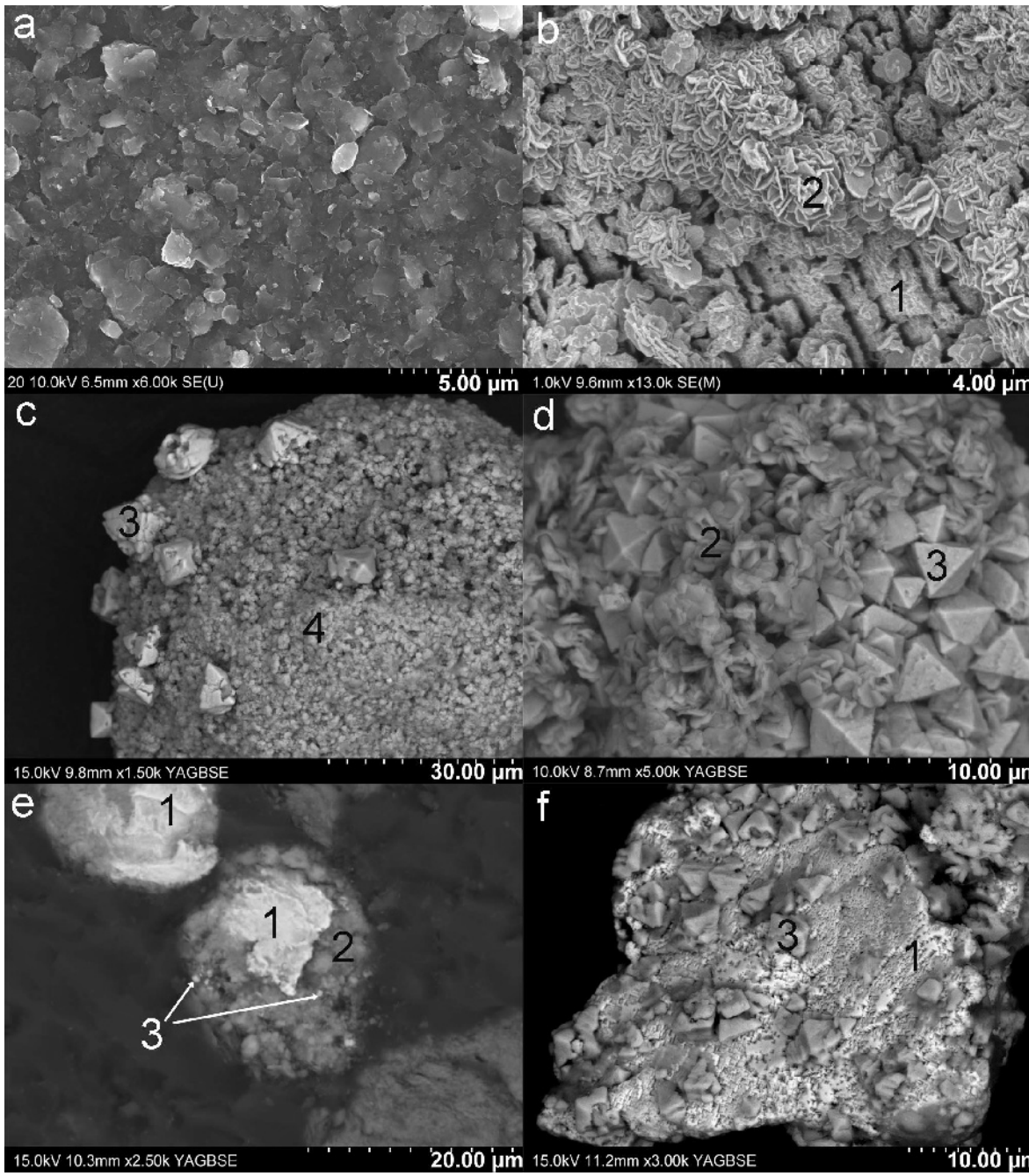

Figure 3. SEM images of (a) CF, (b, c) 1m-Fe, (d) 1m-Fe-CF, (e) 9m-Fe-CF resin embedded sample, and (f) 1m-Fe-CF+pyrite. 1 = metallic iron, 2 = clay particles, 3 = magnetite, 4 = poorly crystalline iron oxides.

https://doi.org/10.1346/CCMN.2015.0630404 Published online by Cambridge University Press

morphology of which differed from that of initial clay particles (Figure 3a), and with an Fe-enrichment in these clay particles indicated by semi-quantitative SEM-EDS analyses; and (3) aggregates with surfaces made entirely of larger magnetite crystals (3 in Figure 3c) and small iron oxides (4 in Figure 3c); type-3 aggregates were less abundant than types 1 and 2.

Examination by TEM of the fine fraction of *x*m-Fe revealed the presence of three types of clay particles: the morphology of the first type was similar to that of initial clays (Figure 4a), the second type displayed filamentous shapes (Figure 4b), and the third type displayed a flaky character and poor crystallinity (Figure D, part a in the supplementary material). Analyses by TEM-EDS revealed Fe enrichment in all three types of clay particles (see the section on 'Chemical analysis of clay particles' below). The filamentous particles were richest in Fe (15.6 at.% of Fe for the particle in Figure 4b) and exhibited an Al:Si atomic ratio of <4, determined from TEM-EDS analyses.

No metallic iron grains were noted during examination by SEM of *x*m-Fe-CF samples. Agglomerates of 10−100 μm, modified phyllosilicates, and well crystallized magnetite crystals were observed (2 and 3, respectively, in Figure 3d). The persistence of metallic iron even in 9m-Fe-CF (1 in Figure 3e) was noted during examination of the resin-embedded preparation which indicates that metallic iron grains were coated systematically by phyllosilicates and/or magnetite.

Examination of the *x*m-Fe-CF samples by TEM revealed no major modification of clay particles' morphologies. In 3m-Fe-CF and 9m-Fe-CF, some Fe-rich particles (up to 17 at.% Fe) displayed a morphological modification with fine needles on their edges (Figure 4c). Such particles were sparse, however, and were not observed in 1m-Fe-CF samples.

In experiments where quartz and calcite were added, these minerals were still observed by SEM in the coarse fraction, irrespective of the presence of iron. No significant modification of quartz- or calcite-grain morphology was noted (not shown). In experiments to which pyrite was added, pyrite grains were not observed directly. In *x*m-CF+pyrite, S-bearing minerals were detected, but being coated with clay particles their actual crystal shape could not be observed and no pure, semi-quantitative spectra were collected, which prevented any unambiguous confirmation of the presence of pyrite. In *x*m-Fe-CF+pyrite, examination by SEM revealed the presence of an iron mono-sulfide, with characteristic rod morphology (Figure D part b, supplementary material). Metallic iron grains were not observed directly in *x*m-Fe-CF+quartz or *x*m-Fe-CF+calcite; as was the case in *x*m-Fe-CF, they were probably covered by magnetite and clay particles. In *x*m-Fe-CF+pyrite, the surface of a few metallic iron grains could be seen, with magnetite crystals on their surface (Figure 3f).

Investigations by TEM revealed morphological changes for some clay particles in all experiments carried out in the presence of metallic iron. For *x*m-Fe-CF+quartz and *x*m-Fe-CF+quartz+calcite, filamentous clay particles were observed after 1 month (Figure 4d) whereas for *x*m-Fe-CF-calcite and *x*m-Fe-CFpyrite, such features were not noted; small stick-shaped structures could be observed but only after 3 months of reaction (Figure 4e). In *x*m-Fe-CF+pyrite, the presence of an iron

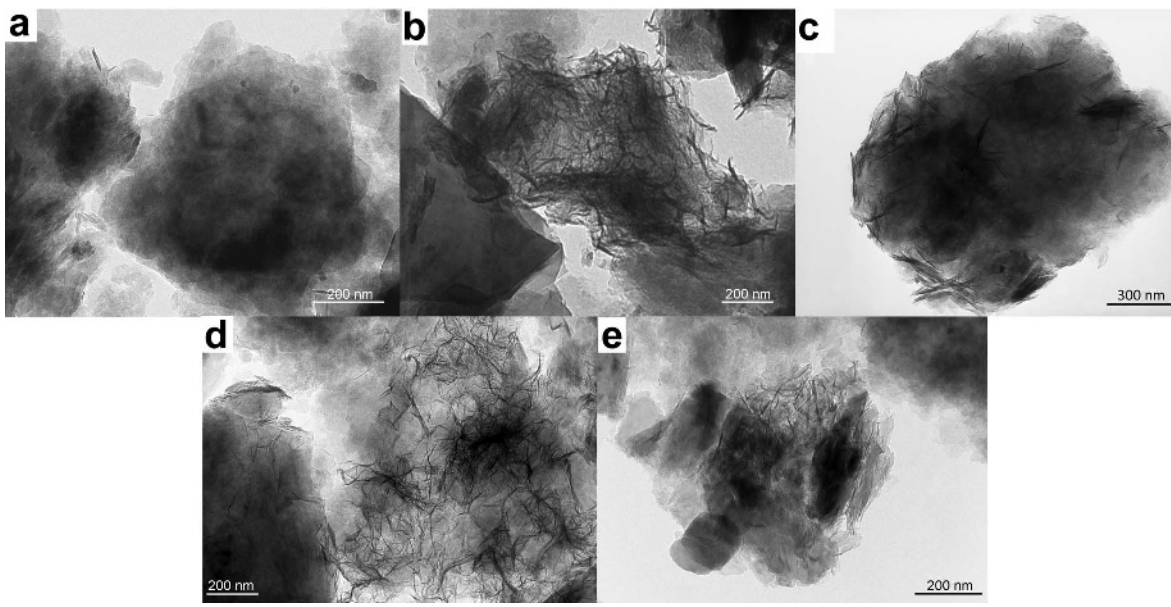

Figure 4. TEM images of: (a) COx clay particles; and (b) end-product clay particles with filamentous shape in 1m-Fe, (c) 9m-Fe-CF, (d) 9m-Fe-CF+quartz, and (e) 9m-Fe-CF+calcite.

https://doi.org/10.1346/CCMN.2015.0630404 Published online by Cambridge University Press

mono-sulfide, with a characteristic rod morphology, was noted by means of TEM examination, as previously observed by SEM (Figure D, part c, supplementary material). The TEM-EDS analyses indicated an Fe:S atomic ratio of close to 1 suggesting that this neoformed phase could be mackinawite.

Determination of textural properties by N_2 adsorption at 77 K. Because samples *x*m-Fe-CF, *x*m-Fe-CF+calcite, and *x*m-Fe-CF+pyrite displayed only minor differences, N_2 adsorption isotherms were only acquired for samples *x*m-Fe (Figure 5a), *x*m-Fe-CF (Figure 5b), and *x*m-Fe-CF+quartz (Figure 5c). The N_2 adsorption-desorption isotherm of COx powder before reaction (Figure 5a) could be classified as a type II isotherm (according to the International Union of Pure and Applied Chemistry classification; Sing *et al.*, 1985) without any marked hysteresis between adsorption and desorption, indicating open porosity between COx particles. The isotherm of sample 9m was superimposed on the initial COx isotherm (Figure 5a) showing the limited impact of experimental procedures (dispersion, heating, centrifugation, freeze-drying) on microstructural properties. In contrast, the adsorption-desorption isotherm corresponding to sample 9m-Fe (Figure 5a) was significantly different and was closer to a type-III isotherm with the formation of a pronounced hysteresis between adsorption and desorption, typical of complex porous networks (Gregg and Sing, 1982). Samples treated for shorter times (*e.g.* 1m-Fe and 3m-Fe) displayed N_2 adsorption-desorption isotherms that were intermediate between those of initial COx and 9m-Fe (Figure E, supplementary material).

Compared to initial COx, the adsorption-desorption isotherm corresponding to the CF sample (Figure 5b) exhibited increased amounts adsorbed, consistent with the greater clay content, as well as a clear hysteresis between adsorption and desorption, that could be attributed tentatively to changes in clay organization resulting from the purification procedure. As in the case of COx, isotherms for samples CF and *x*m-CF were superimposed. Reaction with metallic iron led to textural changes that are significantly different from those observed for COx. Indeed, the adsorption-desorption isotherm corresponding to sample 9m-Fe-CF (Figure 5b) exhibited significantly smaller adsorbed amounts and a nearly absent hysteresis loop.

In the case of the *x*m-CF+quartz samples (Figure 5c), the isotherm displayed a behavior that appeared intermediate between those of samples 9m and 9m-CF, which could be attributed to its intermediate clay content. Reaction with metallic iron led to slightly greater amounts adsorbed and a much more pronounced hysteresis, *i.e.* a behavior that was markedly different from that observed for sample 9m-CF and more like that observed for the sample 9m.

In the absence of metallic iron, no significant time evolution of the SSA of *x*m, *x*m-CF, or *x*m-CF+quartz was observed (Figure 6). In the presence of metallic iron, using an initial value based on the proportion of the various components and assuming negligible SSA for metallic iron and quartz, clear evolutions were revealed. In the case of *x*m-Fe the SSA increased steadily with time from an initial value of 31 m^2/g to 75 m^2/g in 9m-Fe (Figure 6a). The situation is reversed for *x*m-Fe-CF samples, the SSA values of which decreased from 77 to 50 m^2/g in 9m-Fe-CF. In the case of *x*m-Fe-CF+quartz samples, the SSA initially decreased slightly during the first month but increased steadily thereafter to reach a final value of 62 m^2/g after 9 months.

XRD analyses of solid end-products

The XRD patterns (not shown) of the *x*m, *x*m-CF, and *x*m-CF+minerals samples revealed no new crystalline phases, and the initial phases were still present. In contrast, XRD patterns corresponding to samples reacted

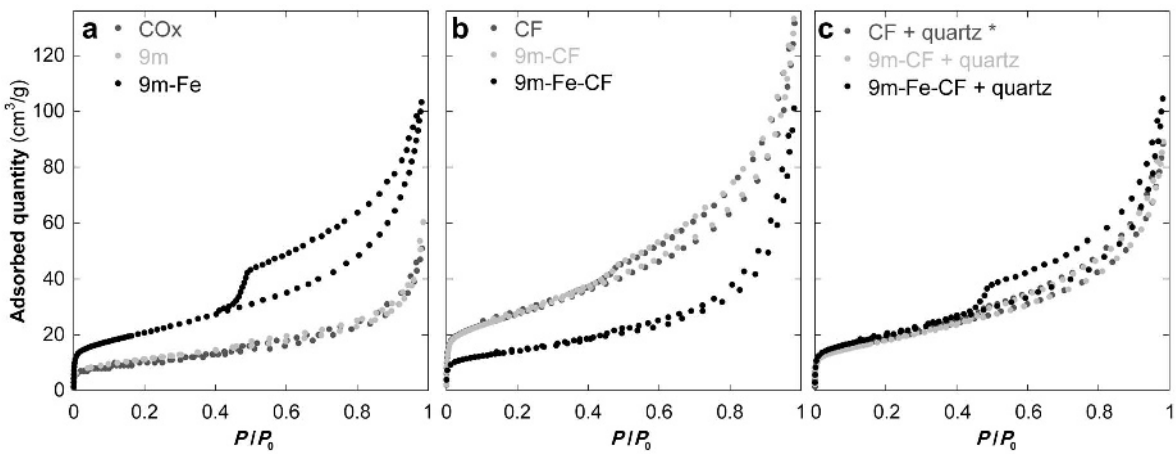

Figure 5. Adsorption-desorption N_2 isotherms of: (a) COx, (b) CF, and (c) CF+quartz before and after reaction, with or without iron. *The values of the 'CF+quartz' isotherm were calculated using 'CF' isotherm values and considering the SSA of quartz to be negligible.

https://doi.org/10.1346/CCMN.2015.0630404 Published online by Cambridge University Press

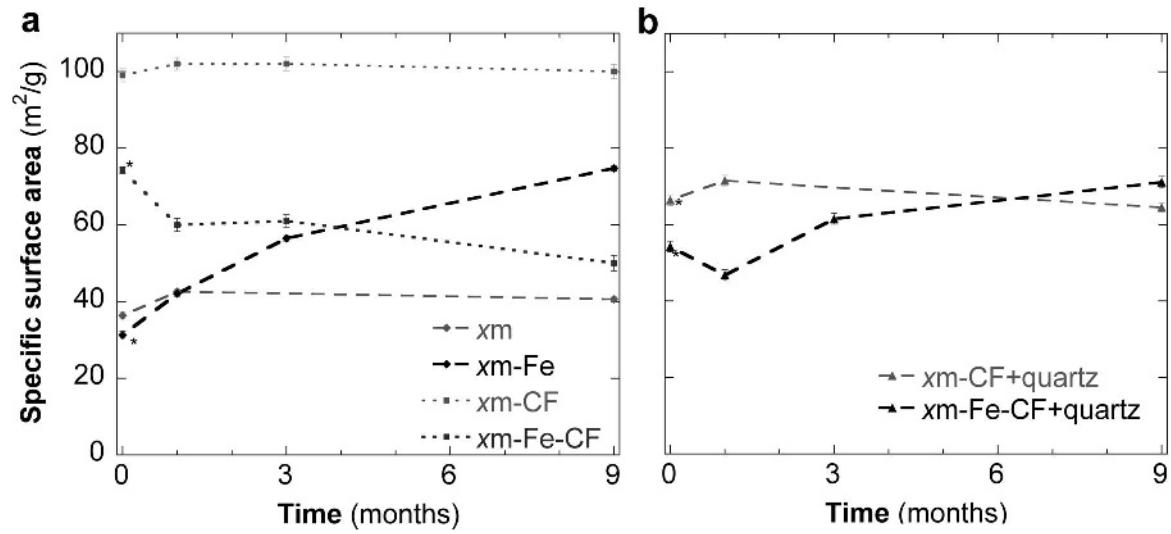

Figure 6. Evolution of SSAs, derived using the BET method, of: (a) COx and CF; and (b) CF + quartz, in the presence and in the absence of metallic iron, as a function of time. The SSAs of the initial mechanical mixtures, indicated with an asterisk, are derived from relative amounts of COx or CF, assuming negligible SSA for metallic iron and quartz.

with metallic iron displayed very significant variations (Figures 7, 8). In the case of COx, after 1 month of reaction, the main metallic iron diffraction peak (110 at 2.03 Å) was reduced significantly (decrease of 69% of the

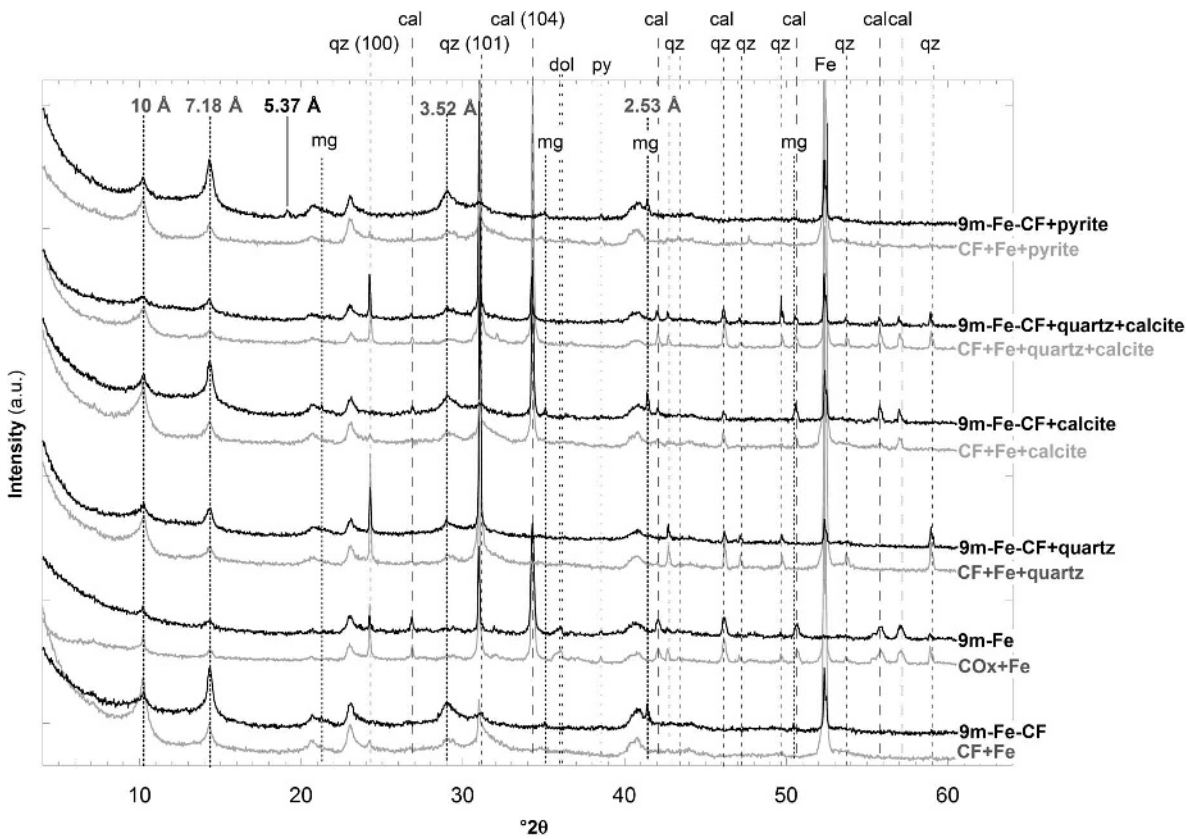

Figure 7. XRD patterns of randomly oriented powders of COx and CF in the presence of metallic iron, with or without the addition of non-clay minerals, before and after 9 months of reaction. Mg = magnetite, qz = quartz, cal = calcite, dol = dolomite, py = pyrite. The diffraction peaks corresponding to the new 7 Å phase (7.18, 3.52, and 2.53 Å) and attributed to an iron sulfide (5.37 Å) are indicated. Unannotated peaks correspond to clay phases.

https://doi.org/10.1346/CCMN.2015.0630404 Published online by Cambridge University Press

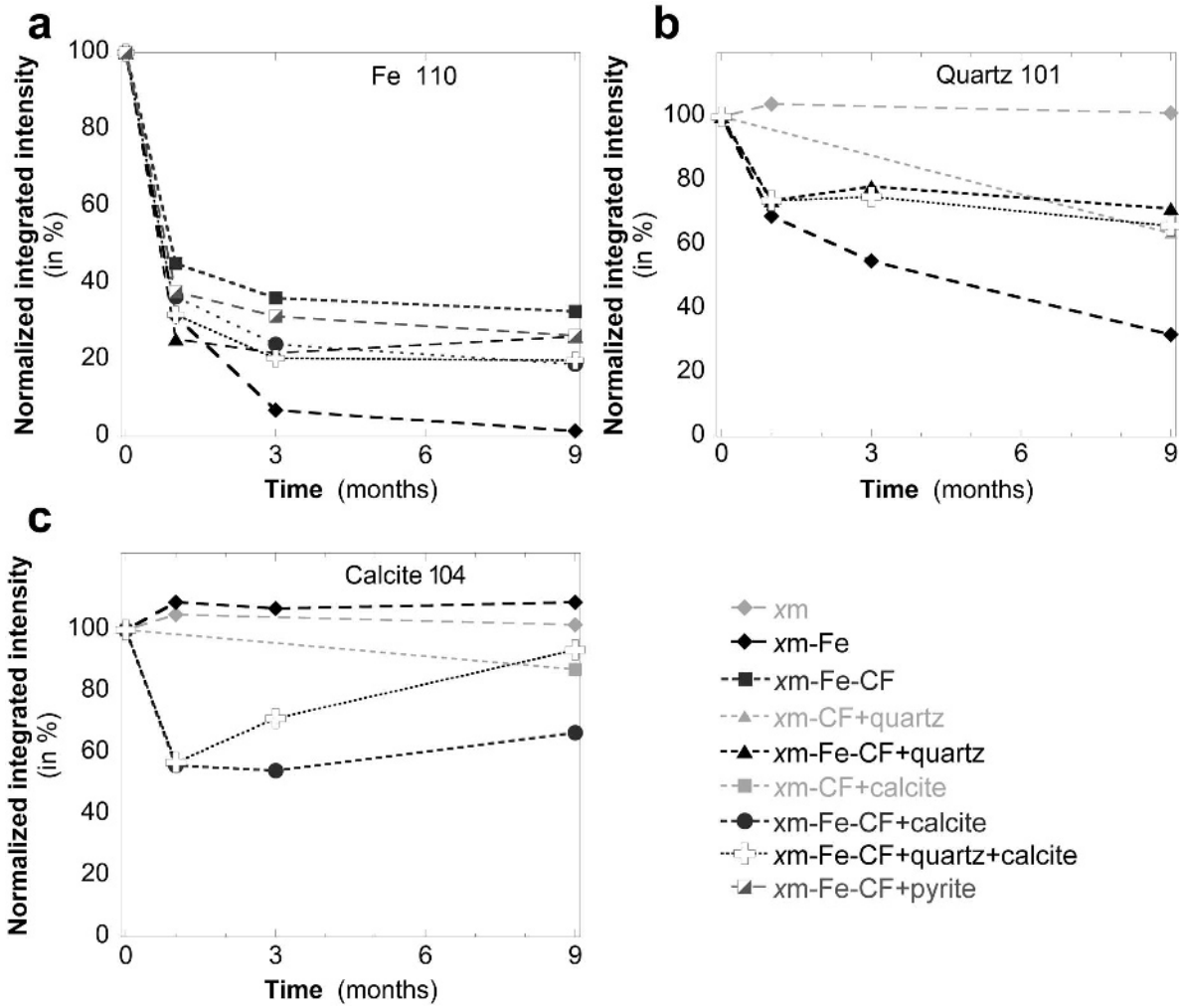

Figure 8. Evolution of the normalized integrated intensities of peaks as a function of time (XRD analyses were conducted in the presence of an internal standard ZnO = 10%). (a) 110 metallic iron peak; (b) 101 quartz peak; and (c) 104 calcite peak. Errors in the values of the normalized intensities are estimated to be <5% for the metallic iron peak and <10% for quartz and calcite peaks.

integrated intensity, Figure 8a). This signal vanished almost completely after 9 months of reaction (Figures 7, 8a). No magnetite was observed after 9 months of reaction, in contrast to the results reported by de Combarieu *et al.* (2007). This difference is probably due to differences in the iron:clay ratio between the two studies (1 for de Combarieu *et al.*, 2007 *vs* 0.16 in the present study), leading to higher pH values and lower Eh values for higher iron:clay ratio. The XRD patterns also revealed a significant decrease in the intensities of quartz diffraction peaks (in 1m-Fe, the intensity corresponded to 69% of the initial intensity and in 9m-Fe, to 32%, Figure 8b) that was not observed in the samples reacted in the absence of iron. In parallel to these changes, which were not linked to any decrease in the intensities corresponding to calcite (Figure 8c), minor modifications of the patterns are noted in the low-angle region (5−15º2θ). In spite of the strong background in this region, a slight decrease in the intensity of 10 Å peaks associated with a small broadening of the 7 Å peak toward lower angles (Figure 7) was noted. Associated with the appearance of faint signals at 3.52 and 2.53 Å, the latter variation could indicate the presence of new Fe-rich 7 Å phases such as berthierine, chamosite-Fe, or odinite (3.52 and 2.53 Å are the second- and the third-order 00*l* peaks). The formation of such phases was reported by de Combarieu *et al.* (2007) for a larger Fe:COx ratio and a smaller amount of kaolinite in the initial sample. Such neoformation could occur to a lesser extent in the present case. No iron carbonates were detected in the present study. The variation of XRD patterns for *x*m-Fe-CF exhibited some differences from the above-mentioned description. After 1 month, metallic iron appeared to have been oxidized significantly (decrease of 55% of the integrated intensity of the main metallic iron peak, Figure 8a); this oxidation appeared to

https://doi.org/10.1346/CCMN.2015.0630404 Published online by Cambridge University Press

diminish over longer time periods, and after 9 months a significant amount of metallic iron could still be observed (36% of the initial intensity, Figure 8). With respect to non-clay minerals, additional information was obtained from these XRD patterns: (1) new peaks corresponding to magnetite were seen in the *x*m-Fe-CF samples (2.53, 2.97, and 4.84 Å); (2) the small amount of quartz remaining after COx purification was dissolved completely in the 1m-Fe-CF sample. The total dissolution of fine quartz grains was confirmed by the XRD pattern collected from the fine-fraction oriented mounts (Figure C, supplementary material) of *x*m-CF (no quartz), compared to COx (quartz present) and 9m-CF (small amounts of quartz present). In the low-angle region, the 10 Å peak was affected significantly (broadening and decrease of the intensity, Figure 7). In the oriented preparations (Figure C, supplementary material), the comparison of ethylene-glycol solvated patterns showed a smaller amount of swelling phases in 9m-Fe-CF than in 9m-CF. These differences indicated either the disappearance of some illite and interlayered illite-smectite or a decrease in their crystallinity. In parallel, the 7 Å peak increased in intensity and broadened on its low-angle side on the powder XRD patterns (Figure 7). The decrease in the 10 Å:7 Å intensity ratio for 9m-Fe-CF in comparison to 9m-CF was also observed in the air-dried and ethylene-glycol solvation patterns (Figure C, supplementary material). This, together with changes at 3.52 and 2.53 Å, indicated clearly the formation of a new Fe-rich 7 Å phase (berthierine, odinite, or chamosite).

Upon addition of various mineral phases, some common trends were observed in the low-angle region, where in all cases the integrated intensity of the 10 Å peak decreased while the intensity of the 7 Å peak increased and new peaks appeared at 3.52, 2.71, and 2.53 Å, indicating the presence of a new 7 Å phase. Some differences were also observed, however. The presence of magnetite was noted in *x*m-Fe-CF+calcite and *x*m-Fe-CF+pyrite samples, through the presence of the peaks at 2.53, 2.97, and 4.84 Å for calcite and at 2.53 and 2.97 Å for pyrite experiments (Figure 7). Magnetite was not detected in the diffraction pattern in experiments carried out in the presence of quartz (*x*m-Fe-CF+quartz and *x*m-Fe-CF+calcite+ quartz). In the specific case of pyrite addition, pyrite was not detected but a new peak at 5.37 Å was observed and attributed to an iron mono-sulfide (Figure 7) in agreement with SEM and TEM observations.

A clear gradation in the consumption of metallic iron was observed by XRD (Figure 8a). COx was the sample in which the most metallic iron by far was oxidized (up to 97%) whereas CF was the sample which displayed the smallest amount of iron consumption (60%). Mineral mixtures displayed intermediate behaviors. The variation of the intensity of quartz (Figure 8b) showed that no quartz was dissolved in COx in the absence of iron, whereas a significant reduction in intensity was observed after reaction. In contrast, in the mineral mixtures where quartz was added, it appeared to be affected both in the presence or absence of metallic iron. The same type of variation was observed in the case of calcite (Figure 8c) intensity which did not vary at all for COx, regardless of the presence of metallic iron, whereas mixtures of CF with calcite displayed a reduction in the calcite intensity both in the presence and absence of metallic iron.

The observations described in the previous paragraphs seemed to indicate that the reference minerals introduced (quartz and calcite) were not entirely stable in the experimental solution at 90ºC, whereas the intrinsic quartz and calcite grains of the COx rock remained stable in solution. This could be attributed either to grain-size effects or to different surface states of quartz and calcite grains. These data must be considered with caution, however. Indeed, because some clay-phase peaks and quartz and calcite peaks were superimposed (101 peak of quartz at 3.34 Å was superimposed on the 003 clay peak; the 100 quartz peak was located in the foot of the 020,110 peaks of the clay phases), the variation of the amount of the clay phases could influence integrated intensity measurements. Furthermore, changes in the mean grain size of the species upon reaction could also influence the intensity of the peak. Larger grains could also be oriented in the sample holder, distorting the measurement. Such orientation effects could explain slight differences in intensity variations of the 101 and 100 quartz peaks in the experiments with the addition of quartz (Figure F, supplementary material).

Determination by HRTEM of neoformed 7 Å phases

Because the nature of the neoformed phyllosilicate (Fe-chlorite or a member of the serpentine family: odinite, cronstedtite, or berthierine) cannot be determined unambiguously by XRD, the interlayer spacings of the clay particles were measured directly by HRTEM. Analyses were performed on 50 particles of samples CF and 3m-Fe-CF+quartz. In CF, no particle with interlayer spacing close to 7 Å was ever observed in spite of the presence of kaolinite in this sample (Figure 9a). The small size of kaolinite particles in comparison to the other clay particles probably explains why they were not observed. In 3m-Fe-CF+quartz, a significant number of 7 Å interlayer distances was measured, with a mean value of 7.3 ± 0.1 Å (Figure 9a). Only one 14 Å particle was observed. Thus, the newly formed species probably belong to the serpentine family. In some cases, 7 and 10 Å phases were observed side by side (Figure 9b).

Chemical analyses of clay particles

Analyses of individual clay particles by TEM-EDS revealed an increase in Fe content after reaction with iron for all of the samples investigated. In the case of COx, mean percentages of 8.4 and 5.8 at.% were recorded for 1m-Fe and 9m-Fe, respectively, whereas

https://doi.org/10.1346/CCMN.2015.0630404 Published online by Cambridge University Press

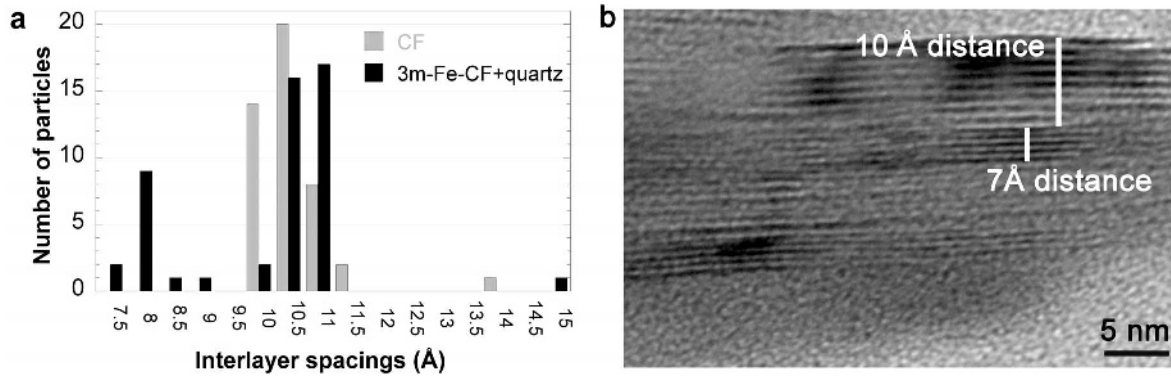

Figure 9. (a) Interlayer distances of clay particles determined by HRTEM: of CF (gray bars) and 3m-Fe-CF+quartz (black bars); (b) HRTEM image with 7 and 10 Å phases side by side in sample 3m-Fe-CF+quartz.

initial particles contained ~2.1 at.% Fe (Table 3). The large standard deviation in such measurements could be attributed to the presence of a few filamentous particles that were very rich in Fe (15.6 at.% for the particle in Figure 4b). Consequently, the difference in Fe contents between 1m-Fe and 9m-Fe may not be truly significant. In any case, dispersion of the results indicated a strong heterogeneity in composition for particles after reaction with metallic iron (Figure 10a). Fe-enrichment appeared to be linked to a decrease in Al content with rather uniform Si content (Figure 10a), which was confirmed by the variation of the Al:Si ratios (0.62 for COx and 0.43 for the 9m-Fe sample, Table 3). Clay-particle compositions appeared to converge toward odinite compositions (simplified formula for odinite according to Bailey, 1988: $(R^{3+}_{1.35}R^{2+}_{1.05}\square_{0.60})(Si_{1.85}Al_{0.15})O_5(OH)_4$, with R^{3+} = Fe or Al, and R^{2+} = Mg, Fe, Ti, or Mn; Al:Si ratio is 0.11–0.25) in the Al–Si–Fe ternary diagram (Figure 10a).

Sample *x*m-Fe-CF also displayed significant Fe enrichment after reaction with metallic iron (Table 3) with relatively large standard deviations and a strong compositional dispersion in the Al-Si-Fe ternary diagram (Figure 10a). In contrast with what was observed for COx, the Si:Al did not evolve significantly upon reaction with metallic iron (Table 3), and the chemical composition did not evolve clearly toward the odinite pole, the Fe-richest particles instead displaying a composition intermediate between odinite, greenalite, and berthierine (Figure 10a).

Experiments with the addition of non-clay-minerals revealed Fe-enrichment in all cases. Two contrasting behaviors were observed, however, in relation to the evolution of the Si:Al ratios. As in the case of CF, the Al:Si ratio remained constant when either pyrite or calcite was added, leading to compositions that were intermediate between odinite, greenalite, and berthierine (Figure 10b). In contrast, for all experiments involving quartz, the Si:Al ratio decreased (as observed for COx) and consequently the compositions of clay particle tended to evolve toward the odinite pole (Figure 10b).

Mössbauer analyses

*x*m-Fe, CF, and *x*m-Fe-CF were characterized by Mössbauer spectroscopy. The Mössbauer spectrum of CF displayed two paramagnetic components corresponding to Fe(III) and Fe(II) in clays (71 and 29%, respectively, Table 4). Thus, in spite of the absence of oxygen suppression during the CF purification procedure, the CF was not oxidized completely. After reaction with

Table 3. Fe atomic percentages and Al:Si atomic ratio in clay particles of COx, CF, and CF with added non-clay minerals, before and after reaction with metallic iron, using TEM-EDS (average over 20 particles).

	Fe percentage (%)				Al:Si ratio			
	Initial	1m-Fe	3m-Fe	9m-Fe	Initial	1m-Fe	3m-Fe	9m-Fe
COx	2.1 ± 1.5*	8.4 ± 4.0	–	5.8 ± 2.8	0.62 ± 0.10	0.43 ± 0.14	–	0.49 ± 0.15
CF	1.6 ± 0.8	4.3 ± 2.4	7.8 ± 3.8	5.7 ± 2.1	0.60 ± 0.10	0.71 ± 0.15	0.59 ± 0.11	0.60 ± 0.11
CF+quartz	–	6.2 ± 2.4	–	7.8 ± 3.9	–	0.57 ± 0.12	–	0.47 ± 0.18
CF+calcite	–	5.5 ± 2.3	–	6.9 ± 2.7	–	0.59 ± 0.13	–	0.58 ± 0.11
CF+quartz+calcite	–	5.5 ± 2.7	–	7.9 ± 2.6	–	0.60 ± 0.14	–	0.48 ± 0.12
CF+pyrite	–	–	–	6.5 ± 2.5	–	–	–	0.60 ± 0.11

(–) not analyzed.
* This large standard deviation is due to the heterogeneity of the clay fraction (the presence, or not, of chlorite particles in the analyzed particles).

https://doi.org/10.1346/CCMN.2015.0630404 Published online by Cambridge University Press

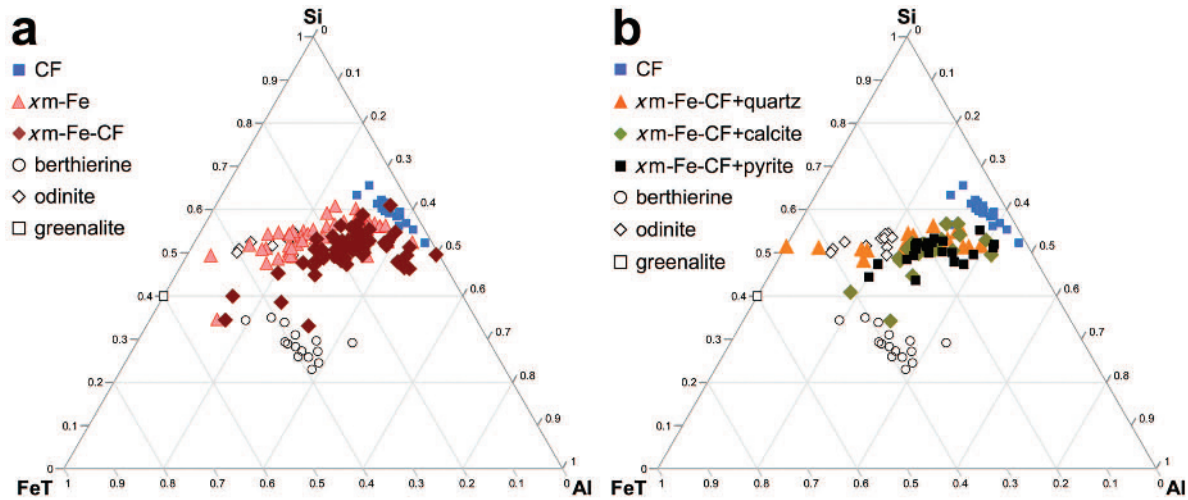

Figure 10. Crystallochemical evolution of clay particles in an Al-Si-FeT (Fe total) ternary diagram (data from TEM-EDS analyses of individual clay particles), in terms of atomic percentage. (a) COx, CF, *x*m-Fe, and *x*m-Fe-CF; (b) CF and *x*m-Fe-CF+mineral. Literature references correspond to berthierine (Brindley, 1982; and Saint-Aubin berthierine), to odinite (Bailey, 1988), and to greenalite (Guggenheim and Bailey, 1989).

Table 4. Mössbauer hyperfine parameters, corresponding attributions, and relative abundance of components of COx and CF end-products.

	IS (mm/s)	QS (mm/s)	H (kOe)	Attribution	Area (%)	Fe(II):Fe(III) ratio in clays
1m-Fe	1.23	2.19	–	Fe(II) VI	23	0.45
	0.34	0.94	–	Fe(III) VI	49	
	0.26	0.43	–	Fe(III) VI	2	
	0	0	330	metallic iron	23	
	0.30	0	475	magnetite IV	1	
	0.63	0	446	magnetite VI	2	
3m-Fe	1.18	2.29	–	Fe(II) VI	25	0.33
	0.33	0.92	–	Fe(III) VI	75	
9m-Fe	1.05	2.55	–	Fe(II) VI	23	0.33
	0.96	2.1	–	Fe(II) VI	2	
	0.38	0.83	–	Fe(III) VI	75	
CF	1.11	2.54	–	Fe(II) VI	29	0.41
	0.32	0.81	–	Fe(III) VI	71	
1m-Fe-CF	1.16	2.47	–	Fe(II) VI	21	0.49
	0.29	0.55	–	Fe(III) VI	43	
	0	0	330	metallic iron	27	
	0.29	0	490	magnetite IV	4	
	0.54	0.33	440	magnetite VI	5	
3m-Fe-CF	1.16	2.44	–	Fe(II) VI	20	0.35
	0.29	0.59	–	Fe(III) VI	57	
	0	0	330	metallic iron	23	
9m-Fe-CF	1.14	2.48	–	Fe(II) VI	35	0.88
	0.33	0.67	–	Fe(III) VI	40	
	0	0	331	metallic iron	16	
	0.31	0	489	magnetite IV	5	
	0.63	0	442	magnetite VI	4	

– Inapplicable
IS: Isomer shift, QS: quadrupole splitting, and H: hyperfine magnetic field
IV: tetrahedral site
VI: octahedral site

https://doi.org/10.1346/CCMN.2015.0630404 Published online by Cambridge University Press

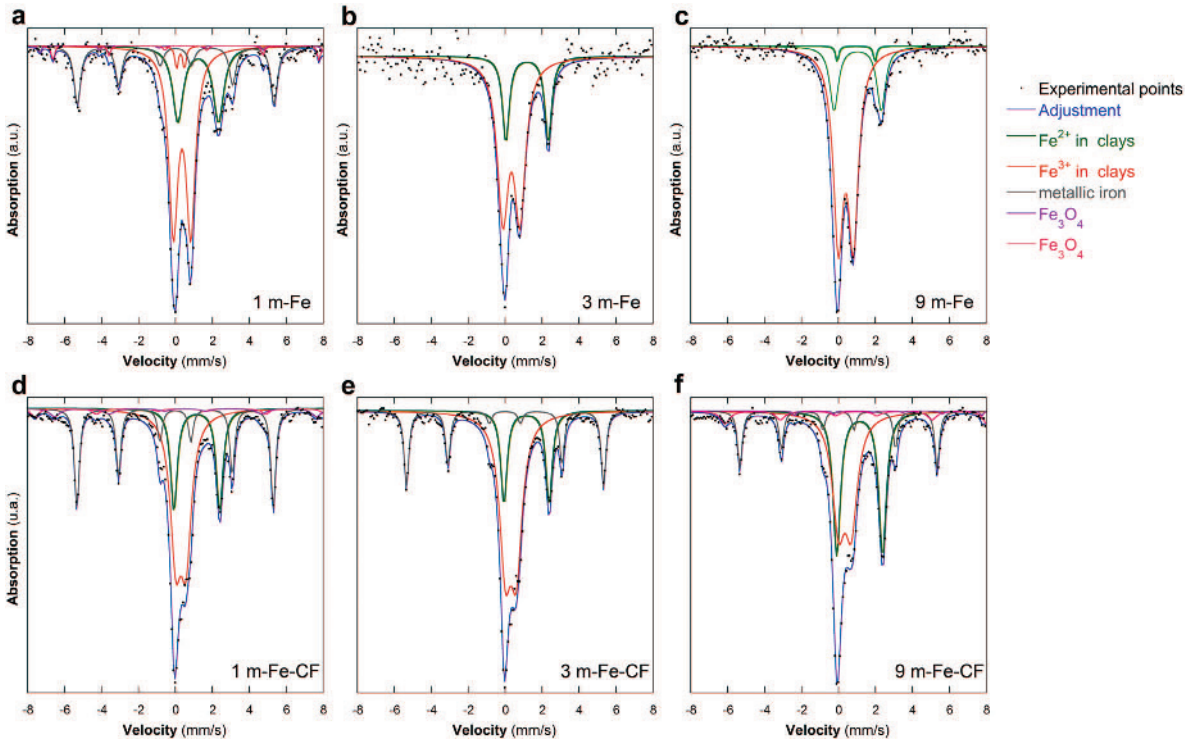

Figure 11. Mössbauer spectra of *x*m-Fe (a–c) and *x*m-Fe-CF (d–f) acquired at room temperature as a function of time.

metallic iron, the Mössbauer spectra of all the samples (Figure 11, Table 4) exhibited a paramagnetic component (quadrupole doublets in clays) in addition to a magnetite and/or metallic iron contribution (sextets). The Mössbauer spectrum of the 1m-Fe sample was fitted with one sextet corresponding to metallic iron (23% of total Fe in the sample) with a hyperfine field (330 kOe) and with two sextets for magnetite with much stronger hyperfine fields (475 and 446 kOe, 3% of total Fe). Fitting the paramagnetic component required use of three doublets corresponding to Fe in octahedral clay layers in the both ferrous (23%) and ferric states (two Fe sites, 51%). The fit of the spectrum with two Fe(III) doublets indicated the presence of two distinct environments for Fe in clays (possibly in two distinct phases). The presence of metallic iron was expected in the 3m-Fe sample in view of XRD analyses (Figure 8a). After 3 and 9 months' reaction, however, neither metallic iron nor magnetite could be detected in the Mössbauer spectra. This discrepancy could be explained by the relatively high signal:noise ratio of the 3m-Fe sample in comparison to those of 1m-Fe and 9m-Fe. In 3m-Fe, fitting was achieved by one doublet for Fe(II) and one doublet for Fe(III), whereas fitting for the 9m-Fe sample required use of one Fe(III) doublet and two Fe(II) doublets. Only a few variations were observed in terms of component fits and the Fe(II):Fe(III) ratio between 1 and 9 months of reaction.

Mössbauer spectra of the *x*m-Fe-CF samples displayed a different evolution. Indeed, in agreement with XRD results, metallic iron appeared to be present in all samples, with only minor decreases in its abundance in samples 3m-Fe-CF and 9m-Fe-CF. The spectral area of the Fe component attributed to magnetite was 9% for 1m-Fe-CF and 9m-Fe-CF. Surprisingly, no Fe bound in the structure of magnetite was detected for 3m-Fe-CF. This is probably due to a stronger background in the 3m-Fe-CF sample compared to the other two. In contrast with the case of COx, all spectra could be fitted using one doublet for Fe(II) and one doublet for Fe(III).

Moreover, the value of the quadrupole splitting of the Fe(III) component was, on average, smaller for CF (0.55, 0.59, and 0.67) than for COx (0.94, 0.43, 0.92, and 0.83). These observations confirmed the different status of iron in these samples already suggested by local chemical analyses (evolution toward a composition intermediate between odinite, greenalite, and berthierine for CF whereas evolution was toward the odinite pole for COx). With increasing reaction time, the Fe(II):Fe(III) ratio evolved toward higher values, except for sample 3m-Fe-CF for which a small decrease was observed. This could be attributed tentatively to the lesser quality of the corresponding spectrum. In any case the 9m-Fe-CF value for this ratio was significantly different from that obtained from 9m-Fe, confirming a different iron chemistry and status in those two samples.

DISCUSSION

With regard to the aims of the present study, it is useful to recall here the main results obtained in studies

https://doi.org/10.1346/CCMN.2015.0630404 Published online by Cambridge University Press

dealing with the interaction of metallic iron with pure clay mineral phases in environmental conditions close to those used in the present study. All the clay minerals present in COx and therefore in its extracted CF (illite, smectite, illite-smectite, and kaolinite) can be destabilized, at varying rates and to various degrees of reaction, upon interaction with metallic iron (Lantenois *et al.*, 2005; Ishidera *et al.*, 2008; Osacky *et al.*, 2010; Lanson *et al.*, 2012; Balko *et al.*, 2012; Perronnet, 2004; Kohler, 2001; Rivard, 2011; Rivard *et al.*, 2013a; 2013b). The reaction involves an important oxidation of metallic iron, a destabilization of clay phases, and the new formation of Fe-rich serpentines and magnetite. Depending on the initial clay mineral, small differences are observed in the precise nature of the neoformed products; kaolinite reaction leads mainly to berthierine and illite, and smectite reaction leads to the precipitation of filamentous or needle-shaped serpentines. In the present study, the evolutions obtained with the extracted CF essentially follow the tendencies observed when smectite or illite, *i.e.* the main clay components of COx, is used. Consequently, the exact nature of the clay minerals involved and their crystal chemistry did not seem to strongly affect the reactions occurring upon their interaction with metallic iron.

In contrast, significant differences were observed between the behavior of COx as a whole and that of its extracted CF, revealing the importance of some of the non-clay minerals in the reaction pathways.

The first difference was in the consumption of iron metal during the reaction. Indeed, the reaction with COx led to almost complete digestion of iron, whereas, in the case of CF, the amount of reacted iron was estimated at ~70% (XRD analyses, Figure 8a). In the latter case (reaction with CF), magnetite was present for all reaction times (XRD results) but not detected in the reaction of COx with metallic iron (Table 5). Under identical experimental conditions, in the absence of any clay, only 56% of metallic iron was oxidized in water to form magnetite (Rivard *et al.*, 2013a). The fact that, in both cases, iron consumption was greater in the presence of clays confirms previous results of Lantenois (2003) and de Combarieu *et al.* (2007). Iron oxidation proceeded through an anodic iron oxidation coupled to a cathodic hydrolysis of water (reactions 1 and 2) which led to the release of H_2 and OH^- resulting in a pH increase and Eh decrease.

$$Fe^0 + 2H_2O = H_2 + 2OH^- + Fe^{2+} \quad (1)$$

$$Fe^0 + 3H_2O = 3/2H_2 + 3OH^- + Fe^{3+} \quad (2)$$

Greater iron consumption could then, in principle, lead to a higher pH. This was not the case here because pH measurements (Figure 1) revealed a higher pH for the *x*m-Fe-CF sample than for the *x*m-Fe sample. This apparent discrepancy can clearly be attributed to a buffering effect in COx. Such buffering was further confirmed by the pH values measured for *x*m samples that are slightly basic and similar to those obtained after reaction with metallic iron. At first sight, it would appear logical to assign this buffering effect to the presence of carbonates. This indeed appeared to be the case before reaction with metallic iron, because the pH values obtained for the *x*m-CF+calcite sample were similar to those obtained for COx. This tendency was much less straightforward in the case of reaction with metallic iron. Indeed, in that case, the pH obtained in *x*m-Fe-CF+calcite samples was close to that obtained for *x*m-Fe-CF samples, *i.e.* significantly higher than that observed for *x*m-Fe samples, in spite of the fact that calcite seemed to have been at least partially destabilized in the *x*m-Fe-CF+calcite samples as evidenced by XRD measurements (Figure 8c). In contrast, and for reaction times with metallic iron $\geqslant$3 months, pH values obtained for *x*m-Fe-CF+quartz samples were the same as those observed for *x*m-Fe samples (Figure 1). Moreover, during the precipitation of magnetite, no significant pH variation was expected, in relation to the consumption of hydroxyls and formation of H_2 (de Combarieu *et al.* 2007). In the present study, lower pH after three months of reaction was not attained for experiments in which magnetite was observed (Figures 1, 7) which means that the precipitation of magnetite did not control the pH. Thus, in the presence of metallic iron, the presence of

Table 5. Neoformed minerals in the three sets of experiments.

	Fe-silicates, Al:Si ratio constant	Fe-silicates, decrease of Al:Si ratio	Fe-carbonates	Magnetite	Fe-sulfide
COx	ε	x	–	ε	–
CF	x	–	–	x	–
CF+quartz	ε	x	–	ε	–
CF+calcite	x	–	–	x	–
CF+quartz+calcite	ε	x	–	ε	–
CF+pyrite	x	–	–	x	x

x: present, ε: very small amount
–: not detected

https://doi.org/10.1346/CCMN.2015.0630404 Published online by Cambridge University Press

quartz appeared to influence the physicochemical parameters of the solution. Such an influence seemed, however, to be effective only at rather small Fe:solid ratios; the rather large Fe:COx ratio used by de Combarieu *et al.* (2007) did not lead to any such effect.

Reactions 1 and 2 also led to the release of Fe in solution. In the present case, as revealed by chemical analyses that displayed extremely small iron contents in solution, all Fe released from metallic iron was incorporated into solid phases. The nature of these solid end-products was significantly different in both cases, however (Table 5). Such differences were not evident in the chemical analyses of solutions. Indeed, in agreement with previous studies (de Combarieu *et al*., 2007), these analyses revealed, both for COx and CF samples, a strong decrease in Ca and Mg concentrations associated with a strong increase in K concentration, which can be attributed to the dissolution of illite and illite-smectite phases (shown by XRD analyses, Figure 7) and to the remobilization of most Mg and some Ca in solid phases. In contrast to analyses of the solutions, most analyses carried out of the solid end-products (SEM, TEM, N_2 adsorption-desorption, TEM-EDS, Mössbauer) indicated significant differences in reactivity between COx and CF. Quantitative EDS analyses (Table 3) showed that the Al:Si ratio was lower in *x*m-Fe clay particles than in initial clay particles, which was not the case for *x*m-Fe-CF particles (Table 3 and 5) for which this ratio remained constant. When plotted in ternary Al/Si/Fe diagrams, *x*m-Fe clay particles converged toward the odinite pole whereas *x*m-Fe-CF particles evolved toward intermediate composition between odinite, greenalite, and berthierine instead (Figure 10a). Mössbauer spectroscopy results also revealed significant differences in quadrupole splitting values of Fe(III) atoms, with larger values for *x*m-Fe than for *x*m-Fe-CF (Table 4); this suggested different Fe siting in the neoformed clay structures. The morphology of the products was also significantly different between the two samples. Fe-rich particles in *x*m-Fe appeared more crystalline than those in *x*m-Fe-CF, with a particularly well developed filamentous habit (Figure 4b,c). These morphological differences were also demonstrated indirectly by N_2 adsorption-desorption experiments. After reaction with metallic iron, *x*m-Fe samples had larger SSAs and there was a marked hysteresis between the adsorption and desorption branches of the isotherm whereas *x*m-Fe-CF exhibited the inverse behavior with smaller SSAs and no hysteresis. The variation in *x*m-Fe samples cannot be attributed to accessory minerals that have very moderate SSA values. The variation in SSA and hysteresis shape must instead be linked to changes in the nature and/or organization of clay particles in the sample that could arise from: (1) the formation of new clay phases with different textural properties; (2) the presence of a greater proportion of clay than in the initial state; or (3) the delamination of the initial clay particles. The XRD results (Figure 7) suggested no increase in the amount of swelling clays, whereas the broadening of the 00l diffraction peak at 10 Å observed after reaction with metallic iron could be indicative of the presence of smaller particles. This, together with the presence in TEM of some less well crystallized particles (flaky bent particles that suggest a limited number of layers per crystallite) favored the existence of delamination processes. As far as *x*m-Fe-CF samples are concerned, the closure of the hysteresis and the decrease of the SSA could be attributed to either a decrease in the amount of swelling clays and/or a modification of the morphology of the clay particles, with formation of more equant particles. No evidence in support of either of these two possibilities was obtained in the present study, however.

The reactivity of COx toward metallic iron appeared to be significantly different from that of its extracted CF. This difference must be attributed to the presence of accessory minerals in COx. As shown in the Results section, the addition of either calcite or pyrite to CF led to only very minor changes in terms of either consumption of iron metal or composition of the final end-products. In particular, in the presence of calcite, no iron carbonates were detected in the end-products, in contrast with results of Martin *et al.* (2008), Schlegel *et al.* (2008, 2010), and de Combarieu *et al.* (2011) which indicated the presence of siderite, or of Schlegel *et al.* (2010) and Pignatelli *et al.* (2014) which indicated the occurrence of chukanovite ($Fe_2CO_3(OH)_2$). This difference can be linked to changes in the availability of carbonate species resulting from different experimental procedures. In the present system (and in those of de Combarieu *et al.*, 2007 and Pierron, 2011, in which no carbonates were observed), the only carbonate source was provided by solid phases, whereas Martin *et al.* (2008) and Schlegel *et al*. (2008, 2010) equilibrated the solution or the whole system with CO_2 or dissolved carbonate. Additional experiments using dolomite instead of calcite (Rivard, 2011) revealed no major changes either. In contrast, after the addition of quartz to CF, the reactivity of the mineral mixtures containing quartz was rather close to that observed with COx. This was illustrated by a greater consumption of iron (Figures 7, 8a), a rather similar particle morphology (Figure 4b,d), a comparable chemistry of the end products with decrease of Al:Si ratios (Tables 3, 5; Figure 10), and an analogous evolution of the N_2 adsorption-desorption isotherms (Figures 5 and 6). In terms of mechanisms, the role of quartz can be described tentatively as follows: high temperature and the increase in pH due to metallic-iron oxidation could activate quartz dissolution, which provided an ancillary source of Si cations added to those extracted from the tetrahedral layer of clays. These Si cations could then participate in the neoformation of Fe-rich clay particles with an Al:Si ratio smaller than in the initial particles (Table 3, 4). This reaction could consume more OH^-

https://doi.org/10.1346/CCMN.2015.0630404 Published online by Cambridge University Press

than the same reaction in the absence of quartz, which could explain the lower final pH value of ~8 (in comparison to 10 in the absence of quartz). The crucial role of pH was further confirmed by the time evolution of the products obtained in experiments involving quartz and CF. Indeed, measurements carried out after 1 month of reaction (1m-Fe-CF+quartz and 1m-Fe-CF+quartz+ calcite samples) revealed a higher pH value (Figure 1). Under these conditions, the Al:Si ratio did not vary (Table 3) and the SSA value decreased. The trends were reversed in samples obtained after 3 and 9 months, in line with a lower pH value of ~8.

These two steps in the evolution could be linked to a delay in quartz dissolution in the case of the *x*m-Fe-CF+quartz sample compared to that of COx. Such a delayed dissolution could be related to the size distribution of quartz grains that may be shifted toward smaller values in natural samples. This is partly supported by the fact that the small amount of <2 μm quartz grains present in CF appeared to be eliminated completely after 1 month. This assumption is also supported partly by additional experiments carried out on non-ground COx (Rivard, 2011) which revealed significantly smaller iron consumption even if in that case no direct links were established between quartz consumption and iron oxidation. Still, such an assumption was not strongly supported by XRD data which show comparable reduction in quartz signals (Figure 8a). More accurate information on that topic could be obtained by carrying out shorter-duration experiments (1 day, 7 days).

Finally, the presence of quartz may have led to an additional precipitation mechanism for Fe-rich serpentines. Indeed, one of the mechanisms of serpentine precipitation that operates in all the experiments corresponded to growth on pre-existing clay layers. Such a mechanism was demonstrated unambiguously in the case of the interaction between kaolinite and metallic iron (Rivard *et al.*, 2013a,b) where berthierine was shown to precipitate epitaxially on the basal planes of kaolinite. Some of the HRTEM images obtained in the present study tended to support the occurrence of similar mechanisms on illite or illite-smectite surfaces (Figure 9b). This appears reasonable considering that the *a* and *b* cell parameters of illite, smectite, and Fe-rich serpentines are similar. In addition to that precipitation mechanism, in the case of pure COx and in experiments carried out with quartz added in CF, TEM images revealed the presence of filamentous particles with rather small Al:Si ratios (<0.4). According to previous studies where metallic iron was reacted with either COx (Pierron, 2011) or smectite (Lantenois *et al.*, 2005; Perronnet *et al.*, 2008; Rivard, 2011), such a shape indicates serpentine precipitation from FeSiAl gels. The presence of additional Si resulting from quartz dissolution could lead to the precipitation of individual filamentous serpentine particles the composition of which was significantly enriched in Fe and Si.

CONCLUSION

Analyses performed on both solutions and solids resulting from the interaction of metallic iron with COx, the extracted CF from COx, and mineral mixtures of CF and the main accessory non-clay minerals of COx revealed some common trends as well as significant differences in reactivity between the different scenarios. In all cases, fast oxidation of metallic iron resulted in an increase in pH and a decrease in Eh which favored the partial dissolution of clay phases. The cations thus extracted combined with Fe leading to the crystallization of Fe-serpentines. In that context, the reactivity of the CF extracted from COx conformed to the results obtained in most previous studies that have investigated the reactivity of pure smectite or smectite-illite phases. Furthermore, the addition of carbonates or pyrite to the CF led to no significant change in reactivity and neither chukanovite nor siderite was ever identified in the present experiments. In contrast, under the conditions used in the present study, *i.e.* for relatively small iron:clay ratios, the presence of quartz appeared to strongly influence the reaction pathway and can be invoked for explaining most of the observed metallic iron reactivity differences between COx and CF. In the presence of quartz, magnetite precipitated only in trace abundances, in contrast to experiments conducted in the absence of quartz, and filamentous serpentine particles were formed with a small Al:Si ratio. Such particles probably formed from an FeSiAl gel that did not seem to exist in the absence of quartz. The increase in reactivity toward metallic iron, in the presence of quartz, could shed new light on some previously obtained results on differences in smectite reactivity. For example, in a study by Perronnet *et al.* (2007), the smectite that exhibits the greatest reactivity also contains opal which is fully dissolved after reaction.

Some details about the exact role of quartz continue to be not fully understood. In particular, the differences observed between the behavior of COx and that of samples of CF+quartz, attributed tentatively to differences in particle-size distribution, require further investigation. Shorter experiments and slightly different Fe:clay ratios might be implemented to obtain additional information. Furthermore, geochemical modeling could be performed using some of the data obtained in the present study to refine some of the proposed mechanisms. The exact nature of the species formed and their crystal chemistry could be analyzed by local spectroscopic techniques such as X-ray absorption spectroscopy and scanning transmission X-ray microscopy. Some of these analyses have been performed and will be the subject of a future publication. Considering the fact that most clay rocks currently considered for radioactive waste disposals contain significant amounts of quartz, the results obtained in the present study should be of significant interest for predicting the long-term behavior of clay barriers in such sites.

https://doi.org/10.1346/CCMN.2015.0630404 Published online by Cambridge University Press

ACKNOWLEDGMENTS

The present research was supported financially by Andra (Agence nationale pour la gestion des déchets radioactifs – the French national radioactive waste management agency). ICP-OES analyses were performed at the Service d'Analyse des Roches et des Minéraux (SARM-CNRS, Vandoeuvre-lès-Nancy, France) and SEM analyses at the Service Commun de Microscopies Electroniques et de Microanalyses (SCMEM, Université de Lorraine, Vandoeuvre-lès-Nancy, France). Special thanks to Yves Moëlo who provided the berthierine sample. Laurent Michot is thanked for improvements to the structure of this manuscript and to the English language.

REFERENCES

Ačai, P., Sorrenti, E., Gorner, T., Polakovic, M., Kongolo, M., and de Donato, P. (2009) Pyrite passivation by acid investigated by inverse liquid chromatography. *Colloids and Surfaces A: Physicochemical and Engineering Aspects*, **337**, 39–46.

Bailey, S.W. (1988) Odinite, a new dioctahedral-trioctahedral Fe^{3+}-rich 1-1 clay mineral. *Clay Minerals*, **23**, 237–247.

Balko, B.A., Bosse, S.A., Cade, A.E., Jones-Landry, E.F., Amonette, J.E., and Daschbach, J.L. (2012) The effect of smectite on the corrosion of iron metal. *Clays and Clay Minerals*, **60**, 136–152.

Beaucaire, C., Tertre, E., Ferrage, E., Grenut, B., Pronier, S., and Madé, B. (2012) A thermodynamic model for the prediction of pore water composition of clayey rock at 25 and 80ºC – comparison with results from hydrothermal alteration experiments. *Chemical Geology*, **334**, 62–76.

Bourdelle, F., Truche, L., Pignatelli, I., Mösser-Ruck, R., Lorgeoux, C., Roszypal, C., and Michau, N. (2014) Iron–clay interactions under hydrothermal conditions: Impact of specific surface area of metallic iron on reaction pathway. *Chemical Geology*, **381**, 194–205.

Brégoin, S. (2003) Variabilité spatiale et temporelle des caractéristiques du Callovo-Oxfordien de Meuse/Haute-Marne. PhD thesis, ENSMP, Paris, 258 pp.

Brindley, G.W. (1982) Chemical compositions of berthierines – A review. *Clays and Clay Minerals*, **30**, 153–155.

Brunauer, S., Emmett, P.H., and Teller, E. (1938) Adsorption of gases in multimolecular layers. *Journal of the American Chemical Society*, **60**, 309–319.

Charpentier, D., Devineau, K., Mosser-Ruck, R., Cathelineau, M., and Villieras, F. (2006) Bentonite-iron interactions under alkaline condition: An experimental approach. *Applied Clay Science*, **32**, 1–13.

de Combarieu, G., Barboux, P., and Minet, Y. (2007) Iron corrosion in Callovo-Oxfordian argillite: From experiments to thermodynamic/kinetic modelling. *Physics and Chemistry of the Earth*, **32**, 346–358.

de Combarieu, G., Schlegel, M.L., Neff, D., Foy, E., Vantelon, D., Barboux, P., and Gin, S. (2011) Glass-iron-clay interactions in a radioactive waste geological disposal: An integrated laboratory-scale experiment. *Applied Geochemistry*, **26**, 65–79.

Gaucher, E., Robelin, C., Matray, J.M., Negral, G., Gros, Y., Heitz, J.F., Vinsot, A., Rebours, H., Cassagnabere, A., and Bouchet, A. (2004) ANDRA underground research laboratory: interpretation of the mineralogical and geochemical data acquired in the Callovian-Oxfordian formation by investigative drilling. *Physics and Chemistry of the Earth*, **29**, 55–77.

Gregg, S.J. and Sing, K.S.W. (1982) *Adsorption, Surface Area and Porosity*. Academic Press, London, pp. 218–228.

Guggenheim, S. and Bailey, S.W. (1989) An occurrence of a modulated serpentine related to the greenalite-caryopilite series. *American Mineralogist*, **74**, 637–641.

Guillaume, D. (2002) Etude expérimentale du système fer – smectite en présence de solution à 80 et 300ºC. PhD thesis, Univ. Henri Poincaré Nancy I, Nancy, France, 211 pp.

Guillaume, D., Neaman, A., Cathelineau, M., Mösser-Ruck, R., Peiffert, C., Abdelmoula, M., Dubessy, J., Villiéras, F., Baronnet, A., and Michau, N. (2003) Experimental synthesis of chlorite from smectite at 300ºC in the presence of metallic Fe. *Clay Minerals*, **38**, 281–302.

Guillaume, D., Neaman, A., Cathelineau, M., Mosser-Ruck, R., Peiffert, C., Abdelmoula, M., Dubessy, J., Villieras, F., and Michau, N. (2004) Experimental study of the transformation of smectite at 80 and 300ºC in the presence of Fe oxides. *Clay Minerals*, **39**, 17–34.

Habert, B. (2000) Réactivité du fer dans les gels et les smectites. PhD thesis, Univ. Paris 6, Paris, 227 pp.

Ishidera, T., Ueno, K., Kurosawa, S., and Suyama, T. (2008) Investigation of montmorillonite alteration and form of iron corrosion products in compacted bentonite in contact with carbon steel for ten years. *Physics and Chemistry of the Earth*, **33**, 269–275.

Jodin-Caumon, M.-C., Mösser-Ruck, R., Randi, A., Pierron, O., Cathelineau, M., and Michau, N. (2010) Mineralogical evolution of a claystone after reaction with iron under thermal gradient. *Clays and Clay Minerals*, **60**, 443–455.

Jodin-Caumon, M.-C., Mösser-Ruck, R., Rousset, D., Randi, A., Cathelineau, M., and Michau, N. (2012) Effect of a thermal gradient on iron-clay interactions. *Clays and Clay Minerals*, **58**, 667–681.

Kohler, E. (2001) *Réactivité des mélanges synthétiques smectite/kaolinite et smectite/aluminium gel en présence d'un excès de fer métal*. DUT Sciences et Génie des Matériaux, Univ. Evry Val d'Essonne, France.

Landais, P. (2006) Advances in geochemical research for the underground disposal of high-level, long-lived radioactive waste in clay formation. *Journal of Geochemical Exploration*, **88**, 32–36.

Lanson, B., Lantenois, S., van Aken, P.A., Bauer, A., and Plançon, A. (2012) Experimental investigation of smectite interaction with metal iron at 80ºC: Structural characterization of newly formed Fe-rich phyllosilicates. *American Mineralogist*, **97**, 864–871.

Lantenois, S. (2003) Réactivité fer métal/smectites en milieu hydraté à 80ºC. PhD thesis, Univ. Orléans, Orléans, France, 225 pp.

Lantenois, S., Lanson, B., Muller, F., Bauer, A., Jullien, M., and Plançon, A. (2005) Experimental study of smectite interaction with metal Fe at low temperature: 1. Smectite destabilization. *Clays and Clay Minerals*, **53**, 597–612.

Martin, F.A., Bataillon, C., and Schlegel, M.L. (2008) Corrosion of iron and low alloyed steel within a water saturated brick of clay under anaerobic deep geological disposal conditions: An integrated experiment. *Journal of Nuclear Materials*, **379**, 80–90.

Mosser-Ruck, R., Cathelineau, M., Guillaume, D., Charpentier, D., Rousset, D., Barres, O., and Michau, N. (2010) Effects of temperature, pH, and iron/clay and liquid/clay ratios on experimental conversion of dioctahedral smectite to berthierine, chlorite, vermiculite, or saponite. *Clays and Clay Minerals*, **58**, 280–291.

Osacký, M., Šucha, V., Czimerova A., and Madejová, J. (2010) Reaction of smectites with iron in a nitrogen atmosphere at 75ºC. *Applied Clay Science*, **50**, 237–244.

Perronnet, M. (2004) Réactivité des matériaux argileux dans un contexte de corrosion métal. Application au stockage des déchets radioactifs en site argileux. PhD thesis, INPL Nancy, France, 280 pp.

Perronnet, M., Villiéras, F., Jullien, M., Razafitianamaharavo,

A., Raynal, J., and Bonnin, D. (2007) Towards a link between the energetic heterogeneities of the edge faces of smectites and their stability in the context of metallic corrosion. *Geochimica et Cosmochimica Acta*, **71**, 1463–1479.

Perronnet, M., Jullien, M., Villieras, F., Raynal, J., Bonnin, D., and Bruno, G. (2008) Evidence of a critical content in Fe(0) on FoCa7 bentonite reactivity at 80ºC. *Applied Clay Science*, **38**, 187–202.

Pierron, O. (2011) Interactions eau-fer-argilite: Rôle des paramètres Liquide/Roche, Fer/Argilite, Température sur la nature des phases minérales. PhD thesis, Univ. H. Poincaré, Nancy, France, 226 pp.

Pignatelli, I., Mugnaioli, E., Hybler, J., Mosser-Ruck, R., Cathelineau, M., and Michau, N. (2013) A multi-technique characterization of cronstedtite synthesized by iron–clay interaction in a step-by-step cooling procedure. *Clays and Clay Minerals*, **61**, 277–289.

Pignatelli, I., Mugnaioli, E., Mosser-Ruck, R., Barres, O., Kolb, U., and Michau, N. (2014) A multi-technique, micrometer- to atomic-scale description of a synthetic analogue of chukanovite, $Fe_2(CO_3)(OH)_2$. *European Journal of Mineralogy*, **26**, 221–229.

Poirier, J.E. (1984) Etudes des mécanismes accompagnant l'adsorption des tensio-actifs ioniques sur les solides, dans le cas des systèmes à interactions faibles : Application à la récupération par voie chimique du pétrole contenu dans les gisements gréseux. PhD thesis, INPL Nancy, France, 328 pp.

Rivard, C. (2011) Contribution à l'étude de la stabilité des minéraux constitutifs de l'argilite du Callovo-Oxfordien en présence de fer à 90ºC. PhD thesis, INPL Nancy, France, 338 pp.

Rivard, C., Pelletier, M., Michau, N., Razafitianamaharavo, A., Bihannic, I., Abdelmoula, M., Ghanbaja, J., and Villiéras, F. (2013a) Berthierine-like mineral formation and stability during the interaction of kaolinite with metallic iron at 90ºC under anoxic and oxidant conditions. *American Mineralogist*, **98**, 163–180.

Rivard, C., Montargès-Pelletier, E., Vantelon, D., Pelletier, M., Karunakaran, C., Michot, L.J., Villiéras, F., and Michau, N. (2013b) Combination of multi-scale and multi-edge X-ray spectroscopy for investigating the products obtained from the interaction between kaolinite and metallic iron in anoxic conditions at 90ºC. *Physics and Chemistry of Minerals*, **40**, 115–132.

Rousset, D. (2002) Etude de la fraction argileuse de séquences sédimentaires de la Meuse et du Gard. Reconstitution de l'histoire diagénétique et des caractéristiques physico-chimiques des cibles. Aspects minéralogiques, géochimiques et isotopiques. PhD thesis, Université Louis Pasteur, Strasbourg, France, 270 pp.

Savage, D., Watson, C., Benbow, S., and Wilson, J. (2010) Modelling iron-bentonite interactions. *Applied Clay Science*, **47**, 91–98.

Schlegel, M.L., Bataillon, C., Benhamida, K., Blanc, C., Menut, D., and Lacour, J.-L. (2008) Metal corrosion and argillite transformation at the water-saturated, high-temperature iron-clay interface: A microscopic-scale study. *Applied Geochemistry*, **23**, 2619–2633.

Schlegel, M.L., Bataillon, C., Blanc, C., Prêt, D., and Eddy, F. (2010) Anodic activation of iron corrosion in clay media under water-saturated conditions at 90ºC: Characterization of the corrosion interface. *Environmental Science & Technology*, **44**, 1503–1508.

Sing, K.S.W., Everett, D.H., Haul, R.A.W., Moscou, L., Pierotti, R.A., Rouquerol, J., and Siemienewska, T. (1985) Reporting physisorption data for gas-solid systems. *Pure and Applied Chemistry*, **57**, 603–619.

Wilson, J., Cressey, G., Cressey, B., Cuadros, J., Ragnarsdottir, K.V., Savage, D., and Shibata, M. (2006) The effect of iron on montmorillonite stability. (II) Experimental investigation. *Geochimica et Cosmochimica Acta*, **70**, 323–336.

Yven, B., Sammartino, S., Géraud, Y., Homand, H., and Villieras, F. (2007) Mineralogy, texture and porosity of Callovo-Oxfordian argillites of the Meuse/Haute-Marne region (Eastern Paris Basin). *Mémoires de la Société Géologique de France*, **178**, 73–90.

(*Received 19 May 2014; revised 31 August 2015; Ms. 879; AE: M.A. Velbel*)